Electronic Supplementary Material (ESI) for Physical Chemistry Chemical Physics.

Supporting Information

Antiferromagnetic Ordering Based on Intermolecular London Dispersion Interactions in Amphiphilic TEMPO Ammonium Salts

Jessica Exner, [a] Steffen Eusterwiemann, [a] Oliver Janka,[b] Carsten Doerenkamp,[c,d] Anja Massolle,[a,e] Oliver Niehaus,[b] Constantin G. Daniliuc,[a] Rainer Pöttgen,*[b] Johannes Neugebauer,*[a,e] Armido Studer,*[a] and Hellmut Eckert,*[c,d]

[a.] *Organic Chemistry Institute, Westfälische Wilhelms-University Münster, Corrensstrasse 40, 48149 Münster, Germany. E-mail: studer@uni-muenster.de*
[b.] *Institut für Anorganische und Analytische Chemie, Westfälische Wilhelms-Universität Münster, Corrensstrasse 30, 48149 Münster, Germany. E-mail: pottgen @uni-muenster.de*
[c.] *Institute of Physical Chemistry, Westfälische Wilhelms-University Münster, Corrensstrasse 28/30, 48149 Münster, Germany. E-mail: eckerth@uni-muenster.de*
[d.] *Institute of Physics, University of São Paulo, Av. Trab. São-Carlense 400, 13566-590 São Carlos (SP), Brazil. E-mail: eckerth@uni-muenster.de*
[e.] *Center for Multiscale Theory and Computation, Corrensstrasse 40, 48149 Münster, Germany. Email: j.neugebauer@uni-muenster.de*

Table of content

1. General Information and Methods

^{1}H NMR, **^{13}C NMR** and **^{19}F NMR** spectra were recorded on a *Bruker DPX 300*, a *Bruker AV 300* or a *Bruker AV 400* spectrometer at RT. The chemical shifts were referred to the solvent residual peak ($CDCl_3$: ^{1}H: δ 7.26 ppm, ^{13}C: δ 77.16 ppm; acetone-d_6: ^{1}H: δ 2.05 ppm, ^{13}C: δ 29.84 ppm; DMSO-d_6: ^{1}H: δ 2.50 ppm, ^{13}C: δ 39.52 ppm) and to an external standard ($CFCl_3$: δ 0.0 ppm) for ^{19}F NMR spectra. Multiplicities of NMR signals are described as s (singlet), d (doublet), t (triplet), q (quartet), p (pentet), sept (septet), m (multiplet) or bs (broad signal). **Mass spectra** (HRMS - ESI) were recorded on a *Finnigan MAT 4200S*, *Bruker Daltonics Micro-TOF*, a *Micromass Quatro LCZ (ESI)* or a *Bruker LTQ Orbitrap XL* and peaks are given in *m/z*. **GC/MS** (EI, 70 eV) was conducted on an *Agilent 6890N* chromatograph with a *HP-5* column combined with a *Waters-Micromass Quatro Micro* spectrometer. Helium (1 bar) was used as a carrier gas and the analysis of the data was executed with *MassLinx 4.0* from *Waters-Micromass*. **IR spectra** were recorded on a *Digilab Varian 3100 FT-IR Excalibur Series* equipped with a *MKII Golden Gate Single Reflection ATR* unit. Recorded IR signals are reported in wavelength (cm^{-1}) with the following abbreviation for the intensity of absorption: *s* (strong), *m* (medium), *w* (weak). **Melting points** (M.p.) were measured on a *Stuart SMP-10* melting point apparatus and are uncorrected. **EPR measurements** were recorded with a *Bruker E-580 ELEXIS EPR spectrometer* (9.4 GHz*,* X-Band, magnetic field of 0.34 T). Solid radicals (T = 5 to 50 K) were measured in thin Borosilicate glasses. The modulation amplitude was set between 1.0 Gauss at a modulation frequency of 100 kHz. Typically, 2048 data points per spectrum at a center field of 337.5 mT and a sweep width of 15 mT with a sweep-time of 167.77s were used. **Magnetic Properties:** The investigated R-DMAT-n radical compounds were used as a polycrystalline powder, waxes or oils and packed in PE capsules. The PE capsules were attached to the sample holder rod of a Vibrating Sample Magnetometer unit (VSM) for measuring the magnetization $M(T,H)$ in a Quantum Design Physical-Property-Measurement-System (PPMS). The samples were investigated in the temperature range of 3-300 K with external magnetic fields up to 80 kOe. **Thin layer chromatography** (TLC) was carried out on *Merck* silica gel 60 F254 plates; detection by UV (irradiation at 254 nm) or dipping into a solution of $KMnO_4$ (1.5 g), $NaHCO_3$ (5.0 g) in H_2O (400 mL), followed by heating. **Flash chromatography** (FC) was performed on silica gel (*Merck*-Si 60: 40 – 63 µm) with a pressure of 0.1 to 0.5 bar. Used eluents are given in parentheses. **Medium Pressure Liquid Chromatography** (MPLC) was used with an automatic flash-system by *Reverleris® IES* from *Grace Davidson* with *Amino Reverleris® cartridges* 4 g oder 12 g) as

stationary phase. In addition to UV-absorption (λ = 254 nm), the detection was carried out by a light scattering detector. **X-Ray diffraction:** For compounds R-DMAT-14-I/OTf and R-DMAT-15-I data sets were collected at 100 K with a *Bruker APEX II CCD* diffractometer. For compounds R-DMAT-15-I/OTf and R-DMAT-16-Cl data sets were collected with a *Bruker D8 Venture PHOTON 100 CMOS* diffractometer at 150 K (R-DMAT-15-I/OTf) and 100 K (R-DMAT-16-Cl). Programs used: data collection: *APEX2 V2014.5-0* (*Bruker AXS* Inc., 2014); cell refinement: *SAINT V8.34A* (*Bruker AXS* Inc., 2013); data reduction: *SAINT V8.34A* (*Bruker AXS* Inc., 2013); absorption correction, *SADABS V2014/2* (*Bruker AXS* Inc., 2014); structure solution *SHELXT-2014* (*Sheldrick*, 2014); structure refinement *SHELXL-2014* (*Sheldrick*, 2014) and graphics, *XP* (*Bruker AXS* Inc., 2014). R-values are given for observed reflections, and wR2 values are given for all reflections.

Exceptions and special features: For compound R-DMAT-15-I a badly disordered solvent molecule (probably one water molecule) was found in the asymmetrical unit and could not be satisfactorily refined. The program *SQUEEZE* (*A.L. Spek, Acta Crystallogr. C,* 2015, ***71***, 9-18) was therefore used to remove mathematically the effect of the solvent. The quoted formula and derived parameters are not included the squeezed solvent molecule. For compound R-DMAT-15-I/OTf one of the two independent molecules found in the asymmetric unit contains a mixture of anion I/OTf in ratio 45/55. For compound R-DMAT-14-I/OTf one of the two independent molecules found in the asymmetric unit contains a mixture of anion I/OTf in ratio 50/50. **Solvents** used for extraction and FC were distilled before use. Et_2O was distilled from K/Na, benzene was distilled from Na, THF was distilled from K, and CH_2Cl_2 was distilled from P_2O_5. **Techniques:** All reactions involving air or moisture sensitive reagents, or intermediates were carried out under argon atmosphere using standard *Schlenk* techniques. All glassware was dried using a heat gun under high vacuum prior to use. Concentration of the reaction mixture was performed under reduced pressure at 40 °C at the appropriate pressure. Purified compounds were further dried under high vacuum. All **reagents** were purchased of the following companies and have been used without further purification: *Acros Organics*, *Sigma-Aldrich*, *Alfa Aesar*, *TCI Germany* or *Merck*.

2. Experimental Procedures

2.1. General Procedures

GP1: General Procedure for the Synthesis of Alkyl Iodides from Alkyl Bromides

According to a literature procedure[1] alkyl bromide (1.0 eq.) was dissolved in acetone (0.6 mL/mmol alkyl bromide), sodium iodide (2.5 eq.) was added and the reaction mixture was stirred at 60 °C for 48 h. After the reaction mixture was allowed to cool to rt, the suspension was filtered and washed with acetone. The solvent was removed *in vacuo* and the residue was dissolved in Et_2O. The solution was washed with $Na_2S_2O_3$ (aq., sat., 2 × 10 mL), NaCl (aq., sat., 2 × 10 mL) and the aqueous layer was extracted with Et_2O. The combined organic layers were dried over $MgSO_4$, the solvent was removed *in vacuo* and the residue was subjected to FC (*n*-pentane) to afford the alkyl iodide.

GP2: General Procedure for the Synthesis of Alkyl Podides from Alkyl Alcohols

According to a literature procedure[2] imidazol (1.2 eq.) and iodine (1.2 eq.) were added to a solution of triphenylphosphine (1.2 eq.) in CH_2Cl_2 (2.8 mL/mmol alkyl alcohol). After addition of alkyl alcohol (1.0 eq.) the reaction mixture was stirred at rt for 1 h. After removal of the solvent *in vacuo*, Et_2O was added to the residue and the suspension was filtered. Then an excess of *n*-pentane was added and the suspension filtered again. The filtrate was washed with $Na_2S_2O_3$ (aq., sat.) and NaCl (aq., sat.) and the aqueous layer was extracted with *n*-pentane. The combined organic layers were dried over $MgSO_4$, the solvent removed *in vacuo* and the crude product was used in the next step without further purification.

GP3: General Procedure for the Synthesis of TEMPO Ammonium Salts (R-DMAT-n)

4-Dimethylamino-TEMPO (1.0 eq.) was added to a solution of alkyl iodide (2.0 eq. – excess) in EtOH (0.7 mL/mmol DMAP) and the reaction mixture was stirred at 80 °C for 24 h. After the reaction mixture was cooled to rt the solvent was removed *in vacuo* and the residue was subjected to MPLC (*Reveleris® Amino 4 g flash cartidges*, 0 min CyHex, 7.5 min 1:1 CyHex/EtOAc, 0 min CH_2Cl_2, 30 min 6:4 CH_2Cl_2/MeOH, 7.5 min 100% MeOH), which gave the TEMPO ammonium salt as an orange solid.

GP4: General Procedure for the Anion Exchange Reaction of R-DMAT Derivatives

A solution of AgX (X = OTf^-, BF_4^-, PF_6^-, SbF_6^-, 1.0 eq.) in acetone (10 mL/mmol) was added at rt to a solution of a TEMPO ammonium salt (1.0 eq.) in acetone (10 mL/mmol) within 5 min and the reaction mixture was stirred for 5 to 10 min. After filtration of the suspension and removal of the solvent in vacuo the residue was subjected to MPLC (*Reveleris® Amino 4 g flash cartidges*, 0 min CyHex, 7.5 min 1:1 CyHex/EtOAc, 0 min CH_2Cl_2, 30 min 6:4 CH_2Cl_2/MeOH, 7.5 min 100% MeOH), which afforded the TEMPO ammonium salt as an orange solid.

2.2. Synthesis of Radical Precursor Compounds

4-Oxo-TEMPO[3]

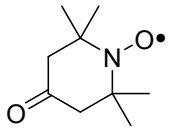

$C_9H_{16}NO_2^•$
170.23 g/mol

At 0 °C H_2O_2 (12 mL, aq., 50%, 105 mmol, 3.26 eq.) was added dropwise to a solution of 2,2,6,6-tetramethylpiperidin-4-one (5.00 g, 32.2 mmol, 1.0 eq.) and Na_2WO_4 (398 mg, 1.36 mmol, 4.0 mol%) in H_2O (25 mL). The reaction mixture was allowed to warm to rt and stirred for 24 h. After addition of brine (10 mL) the aqueous layer was extracted with MTBE (3 × 30 mL). The combined organic layers were dried over $MgSO_4$ and the solvent was removed *in vacuo*. FC (*n*-pentane/acetone 10:1) afforded the title compound (4.66 g, 27.4 mmol, 85%) as a red solid.

IR (ATR, neat): 3487 *br w*, 2977*m*, 1719*s*, 1638*w*, 1466*w*, 1366*m*, 1313*m*, 1232*s*, 1062*w*, 686*w*; **HRMS** (ESI, positive mode): *m/z* = 193.1073 calculated for $[M+Na]^+$, found: 193.1037.

4-Dimethylamino-TEMPO[4]

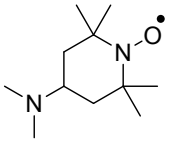

$C_{11}H_{23}N_2O^•$
199.31 g/mol

4-Oxo-TEMPO (2.55 g, 15.0 mmol, 1.0 eq.) and $Ti(OiPr)_4$ (5.12 g, 5.33 mL, 18.0 mmol, 1.2 eq.) were dissolved in THF (3.0 mL) and stirred at rt for 30 min. Dimethylammoniumhydrochloride (2.45 g, 30.0 mmol, 2.0 eq.) was added and the reaction mixture stirred at rt for 2.5 h. After addition of EtOH (10 mL) and $NaBH_4$ (851 mg, 22.5 mmol, 1.5 eq.) at 0 °C, the reaction mixture was allowed to warm to rt and stirring was continued for 24 h at that temperature. Then $NaHCO_3$ (aq., sat., 6.0 mL) was added and the suspension filtered over *Celite®* and washed with EtOAc and MeOH. After removal of the solvent *in vacuo*, FC (CH_2Cl_2/MeOH 15:1) afforded the title compound (1.18 g, 5.94 mmol, 79%) as a red solid.

IR (ATR, neat): 3403*w*, 2976*m*, 2340*m*, 2711*w*, 1692*m*, 1464*m*, 1377*s*, 1242*w*, 1122*s*, 1023*w*, 930*w*, 865*w*, 675*w*; **HRMS** (ESI): *m/z* = 200.1883 calculated for $[M+H]^+$, found: 200.1891.

2.3. Synthesis of Alkyl Iodides

1-Iodoundecane

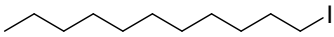

$C_{11}H_{23}I$
282.20 g/mol

According to GP2 with triphenylphosphine (1.83 g, 6.96 mmol, 1.2 eq.), imidazol (474 mg, 6.96 mmol, 1.2 eq.), iodine (1.77 g, 6.96 mmol, 1.2 eq.) and 1-undecanol (1.00 g, 1.20 mL, 5.80 mmol, 1.0 eq.) the title compound (1.58 g, 5.60 mmol, 96%) was obtained as a colorless oil, which was used in the next step without further purification. Spectroscopic data are in accordance with those described in the literature.[5]

^{1}H NMR: (300 MHz, $CDCl_3$) δ (ppm) = 3.19 (t, *J* = 7.0 Hz, 2H, ICH_2), 1.81 (p, *J* = 7.0 Hz, 2H, CH_2), 1.43 – 1.21 (s, 16H, CH_2), 0.92 – 0.83 (m, 3H, CH_3); **^{13}C NMR** (75 MHz, $CDCl_3$) δ (ppm) = 33.8 (ICH_2), 32.1 (CH_2), 30.7 (CH_2), 29.7 (CH_2), 29.7 (CH_2), 29.6 (CH_2), 29.6 (CH_2), 28.7 (CH_2), 22.8 (CH_2), 14.3 (CH_2), 7.4 (CH_3); **GC/MS** (EI): *m/z* = 282.2 calculated for $[M]^+$, found: 282.2.

1-Iodododecane

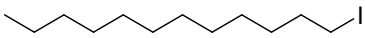

$C_{12}H_{25}I$
296.23 g/mol

According to GP2 with triphenylphosphine (1.70 g, 6.50 mmol, 1.2 eq.), imidazol (450 mg, 6.50 mmol, 1.2 eq.), iodine (1.65 g, 6.50 mmol, 1.2 eq.) and 1-dodecanol (1.00 g, 5.40 mmol, 1.0 eq.) the title compound (1.51 g, 5.09 mmol, 95%) was obtained as a colorless oil, which was used in the next step without further purification. Spectroscopic data are in accordance with those described in the literature.[6]

^{1}H NMR (300 MHz, $CDCl_3$): δ (ppm) = 3.19 (t, *J* = 7.1 Hz, 2H, ICH_2), 1.82 (p, *J* = 7.1 Hz, 2H, CH_2), 1.26 (s, 18H, CH_2), 0.91 – 0.85 (m, 3H, CH_3); **^{13}C NMR** (75 MHz, $CDCl_3$) δ (ppm) = 33.8 (ICH_2), 32.1 (CH_2), 30.7 (CH_2), 29.8 (2 x CH_2), 29.7 (CH_2), 29.6 (CH_2), 29.5 (CH_2), 28.7 (CH_2), 22.8 (CH_2), 14.3 (CH_2), 7.4 (CH_3); **GC/MS** (EI): *m/z* = 296.1 calculated for $[M]^+$, found: 296.1.

1-Iodotridecane

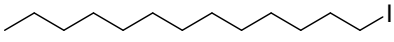

$C_{13}H_{27}I$
310.26 g/mol

The title compound was obtained according to GP1 with 1-bromotridecane (500 mg, 1.90 mmol, 1.0 eq.) and sodium iodide (712 mg, 4.75 mmol, 2.5 eq.) in acetone at 60 °C for 48 h. FC (*n*-pentane) afforded the title compound (576 mg, 1.86 mmol, 98%) as a colorless liquid. Spectroscopic data are in accordance with those described in the literature.[7]

^{1}H NMR (300 MHz, $CDCl_3$): δ (ppm) = 3.19 (t, *J* = 7.1 Hz, 2H, ICH_2), 1.82 (p, *J* = 7.1 Hz, 2H, CH_2), 1.26 (s, 20H, CH_2), 0.91 – 0.85 (m, 3H, CH_3); **^{13}C NMR** (75 MHz, $CDCl_3$) δ (ppm) = 33.8 (ICH_2),

32.1 (*C*H$_2$), 30.7 (*C*H$_2$), 29.8 (*C*H$_2$), 29.8 (*C*H$_2$), 29.8 (*C*H$_2$), 29.7 (*C*H$_2$), 29.6 (*C*H$_2$), 29.5 (*C*H$_2$), 28.7 (*C*H$_2$), 22.8 (*C*H$_2$), 14.3 (*C*H$_2$), 7.4 (*C*H$_3$); **GC/MS** (EI): *m/z* = 310.1 calculated. for [M]$^+$, found: 310.1.

1-Iodotetradecane

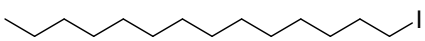

$C_{14}H_{29}I$
324.28 g/mol

According to GP2 with triphenylphosphine (1.50 g, 5.60 mmol, 1.2 eq.), imidazol (380 mg, 5.60 mmol, 1.2 eq.), iodine (1.40 g, 5.60 mmol, 1.2 eq.) and 1-tetradecanol (1.00 g, 4.70 mmol, 1.0 eq.) the title compound (1.33 g, 4.10 mmol, 88%) was obtained as a colorless oil, which was used in the next step without further purification. Spectroscopic data are in accordance with those described in the literature.[8]

^{1}H NMR (300 MHz, $CDCl_3$): δ (ppm) = 3.19 (t, *J* = 7.1 Hz, 2H, IC*H*$_2$), 1.82 (p, *J* = 7.1 Hz, 2H, C*H*$_2$), 1.26 (s, 22H, C*H*$_2$), 0.91 – 0.85 (m, 3H, C*H*$_3$); **^{13}C NMR** (75 MHz, $CDCl_3$) δ (ppm) = 33.8 (I*C*H$_2$), 32.1 (*C*H$_2$), 30.7 (*C*H$_2$), 29.8 (*C*H$_2$), 29.8 (*C*H$_2$), 29.8 (2 x *C*H$_2$), 29.7 (*C*H$_2$), 29.6 (*C*H$_2$), 29.5 (*C*H$_2$), 28.7 (*C*H$_2$), 22.9 (*C*H$_2$), 14.3 (*C*H$_2$), 7.4 (*C*H$_3$); **GC/MS** (EI): *m/z* = 324.1 calculated. for [M]$^+$, found: 324.1.

1-Iodopentadecane

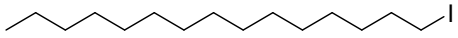

$C_{15}H_{31}I$
338.31 g/mol

The title compound was obtained according to GP1 with 1-bromopentadecane (500 mg, 1.70 mmol, 1.0 eq.) and sodium iodide (637 mg, 4.25 mmol, 2.5 eq.) in acetone at 60 °C for 48 h. FC (*n*-pentane) afforded the title compound (540 mg, 1.56 mmol, 93%) as a colorless liquid. Spectroscopic data are in accordance with those described in the literature.[9]

^{1}H NMR (300 MHz, $CDCl_3$): δ (ppm) = 3.19 (t, *J* = 7.1 Hz, 2H, IC*H*$_2$), 1.82 (p, *J* = 7.1 Hz, 2H, C*H*$_2$), 1.26 (s, 24H, C*H*$_2$), 0.91 – 0.85 (m, 3H, C*H*$_3$); **^{13}C NMR** (75 MHz, $CDCl_3$) δ (ppm) = 33.8 (I*C*H$_2$), 32.1 (*C*H$_2$), 30.7 (*C*H$_2$), 29.9 (*C*H$_2$), 29.9 (*C*H$_2$), 29.8 (*C*H$_2$), 29.8 (2 x *C*H$_2$), 29.7 (*C*H$_2$), 29.6 (*C*H$_2$), 29.5 (*C*H$_2$), 28.7 (*C*H$_2$), 22.9 (*C*H$_2$), 14.3 (*C*H$_2$), 7.4 (*C*H$_3$); **GC/MS** (EI): *m/z* = 338.1 calculated for [M]$^+$, found: 338.1.

1-Iodoheptadecane

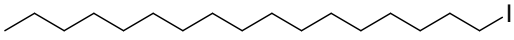

$C_{17}H_{35}I$
366.36 g/mol

The title compound was obtained according to GP1 with 1-bromoheptadecane (500 mg, 1.57 mmol, 1.0 eq.) and sodium iodide (587 mg, 3.91 mmol, 2.5 eq.) in acetone at 60 °C for 48 h. FC (*n*-pentane) afforded the title compound (494 mg,

1.35 mmol, 86%) as a colorless crystalline solid. Spectroscopic data are in accordance with those described in the literature.[10]

^{1}H NMR (300 MHz, $CDCl_3$): δ (ppm) = 3.19 (t, *J* = 7.1 Hz, 2H, ICH_2), 1.82 (p, *J* = 7.1 Hz, 2H, CH_2), 1.26 (s, 28H, CH_2), 0.91 – 0.85 (m, 3H, CH_3); **^{13}C NMR** (75 MHz, $CDCl_3$) δ (ppm) = 33.8 (ICH_2), 32.1 (*C*H_2), 30.7 (*C*H_2), 29.9 (3 x *C*H_2), 29.8 (3 x *C*H_2), 29.8 (*C*H_2), 29.7 (*C*H_2), 29.6 (*C*H_2), 29.5 (*C*H_2), 28.7 (*C*H_2), 22.9 (*C*H_2), 14.3 (*C*H_2), 7.4 (*C*H_3); **GC/MS** (EI): *m/z* = 366.1783 calculated for $[M]^+$, found: 366.3.

Hexadecyltriflate

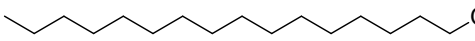

$C_{17}H_{33}F_3O_3S$
374.50 g/mol

In accordance to a literature procedure[11] Tf_2O (0.64 mL, 3.80 mmol, 1.9 eq.) was added at 0 °C to a solution of 2,6-lutidine (0.44 mL, 3.8 mmol, 1.9 eq.) in CH_2Cl_2 (4.5 mL) within 10 min. Hexadecylalcohol (485 mg, 2.00 mmol, 1.0 eq.) was added at 0 °C and the reaction mixture was stirred at rt for 1 h. After addition of H_2O (20 mL) the reaction mixture was extracted with CH_2Cl_2 (2 × 20 mL), the combined organic layers were washed with HCl (aq., 1 M, 10 mL) and $NaHCO_3$ (aq., sat., 10 mL) and dried over $MgSO_4$. The solvent was removed *in vacuo* and the residue subjected to FC (*n*-pentane/MTBE 5:1), which afforded the title compound (712 mg, 1.90 mmol, 95%) as a colorless solid. Spectroscopic data are in accordance with those described in the literature.[12]

^{1}H NMR (300 MHz, $CDCl_3$) δ (ppm) = 4.53 (*t*, *J* = 6.5 Hz, 2H, CH_2), 1.90 – 1.76 (*m*, 2H, CH_2), 1.46 – 1.38 (*m*, 2H, CH_2), 1.26 (*s*, 24H, CH_2), 0.92 – 0.84 (*m*, 3H, CH_3); **^{13}C NMR** (75 MHz, $CDCl_3$) δ (ppm) = 118.8 (*d*, $^1J_{C\text{-}F}$ = 319.6 Hz, *C*F_3), 77.8 (*C*H_2), 32.1 (*C*H_2), 29.8 (*C*H_2), 29.8 (*C*H_2), 29.8 (*C*H_2), 29.8 (*C*H_2), 29.8 (*C*H_2), 29.7 (*C*H_2), 29.6 (*C*H_2), 29.5 (*C*H_2), 29.5 (*C*H_2), 29.4 (*C*H_2), 29.0 (*C*H_2), 25.2 (CH_2), 22.8 (*C*H_2), 14.2 (*C*H_3); **^{19}F NMR** (282 MHz, $CDCl_3$) δ (ppm) = –74.9 (C*F*$_3$).

2.4. Synthesis of R-DMAT-n Systems with Iodide as a Counter Anion (n = 1-18)

N-Methyl-1-oxyl-*N,N*,2,2,6,6-hexamethylpiperidin-4-ammonium-iodide (R-DMAT-1)[13]

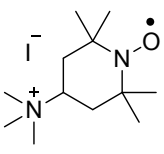

$C_{12}H_{26}IN_2O^{\bullet}$
341.25 g/mol

The title compound was synthesized according to GP3 with 4-dimethylamino-TEMPO (177 mg, 888 μmol, 1.0 eq.) and methyl iodide (200 μL, 3.20 mmol, 3.6 eq.) in EtOH (1.5 mL) at 80 °C for 24 h. MPLC afforded the title compound as an orange solid (201 mg, 589 μmol, 66%).

M.p.: 226 °C; **IR** (ATR, neat): 3425*br s*, 2971*m*, 1659*m*, 1622*m*, 1476*m*, 1360*m*, 1239*s*, 1181*s*, 1106*w*, 971*m*, 890*s*, 845*w*, 671*m*; **HRMS** (ESI, positive mode): *m/z* = 214.2040 calculated for $[M\text{-}I^-]^+$, found: 214.2076.

N-Ethyl-1-oxyl-*N,N*,2,2,6,6-hexamethylpiperidin-4-ammonium-iodide (R-DMAT-2)

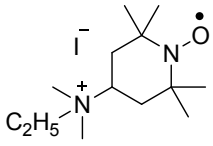

$C_{13}H_{28}IN_2O^{\bullet}$
355.28 g/mol

The title compound was synthesized according to GP3 with 4-dimethylamino-TEMPO (199 mg, 998 μmol, 1.0 eq.) and ethyl iodide (180 μL, 2.26 mmol, 2.0 eq.) in EtOH (1.3 mL) at 80 °C for 24 h. MPLC afforded the title compound as an orange solid (330 mg, 929 μmol, 93%).

M.p.: decomposition at 205 °C; **IR** (ATR, neat): 2974*m*, 1689*s*, 1622*m*, 1465*m*, 1386*s*, 1246*m*, 1180*m*, 1103*w*, 814*w*; **HRMS** (ESI, positive mode): *m/z* = 228.2196 calculated for $[M\text{-}I^-]^+$, found: 228.2211.

N-Propyl-1-oxyl-*N,N*,2,2,6,6-hexamethylpiperidin-4-ammonium-iodide (R-DMAT-3)

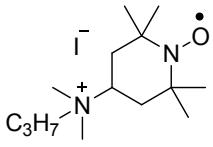

$C_{14}H_{30}IN_2O^{\bullet}$
369.31 g/mol

The title compound was synthesized according to GP3 with 4-dimethylamino-TEMPO (100 mg, 0.502 mmol, 1.0 eq.) and 1-iodopropane (98 μl, 1.0 mmol, 2.0 eq.) in EtOH (0.70 mL) at 80 °C for 24 h. MPLC afforded the title compound as an orange solid (134 mg, 363 μmol, 73%).

M.p.: decomposition at 207 °C; **IR** (ATR, neat): 2972*w*, 1671*s*, 1480*m*, 1199*s*, 1182*s*, 831*w*, 720*m*; **HRMS** (ESI, positive mode): *m/z* = 242.2353 calculated for $[M\text{-}I^-]^+$, found: 242.2323.

N-Butyl-1-oxyl-*N,N*,2,2,6,6-hexamethylpiperidin-4-ammonium-iodide (R-DMAT-4)

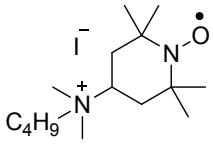

$C_{15}H_{32}IN_2O^{\bullet}$
383.33 g/mol

The title compound was synthesized according to GP3 with 4-dimethylamino-TEMPO (100 mg, 0.502 mmol, 1.0 eq.) and 1-iodobutane (185 mg, 1.00 mmol, 2.0 eq.) in EtOH (0.70 mL) at 80 °C for 24 h. MPLC afforded the title compound as an orange solid (139 mg, 363 μmol, 73%).

M.p.: 114 °C; **IR** (ATR, neat): 3458br s, 2971m, 1689w, 1465*s*, 1367m, 1243s, 1179m, 1179s, 888m, 677w; **HRMS** (ESI, positive mode): *m/z* = 256.2509 calculated for $[M\text{-}I^-]^+$, found: 256.2521.

N-Pentyl-1-oxyl-*N,N*,2,2,6,6-hexamethylpiperidin-4-ammonium-iodide (R-DMAT-5)

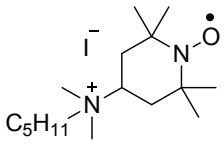

$C_{16}H_{34}IN_2O^{\bullet}$
397.36 g/mol

The title compound was synthesized according to GP3 with 4-dimethylamino-TEMPO (199 mg, 998 μmol, 1.0 eq.) and 1-iodopentane (0.26 mL, 2.0 mmol, 2.0 eq.) in EtOH (1.3 mL) at 80 °C for 24 h. MPLC afforded the title compound as an orange solid (382 mg, 961 μmol, 96%).

M.p.: 158 °C; **IR** (ATR, neat): 2955*s*, 2869*m*, 1667*w*, 1472*s*, 1241*s*, 1186*s*, 1109*w*, 1047*w*, 969*w*, 896*s*, 842*m*, 785*w*, 731*w*, 677*m*; **HRMS** (ESI, positive mode): *m/z* = 270.2666 calculated for $[M\text{-}I^-]^+$, found: 270.2679.

N-Hexyl-1-oxyl-*N,N*,2,2,6,6-hexamethylpiperidin-4-ammonium-iodide (R-DMAT-6)

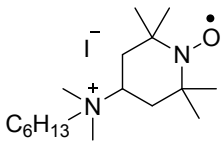

$C_{17}H_{36}IN_2O^{\bullet}$
411.39 g/mol

The title compound was synthesized according to GP3 with 4-dimethylamino-TEMPO (100 mg, 0.502 mmol, 1.0 eq.) and 1-iodohexane (148 μL, 1.00 mmol, 2.0 eq.) in EtOH (0.70 mL) at 80 °C for 24 h. MPLC afforded the title compound as an orange oil (133 mg, 323 μmol, 64%).

IR (ATR, neat): 2931*m*, 1685m, 1675m, 1465m, 1243m, 1200s, 1177s, 1131m, 719m; **HRMS** (ESI, positive mode): *m/z* = 284.2822 calculated for $[M\text{-}I^-]^+$, found: 284.2834.

N-Heptyl-1-oxyl-*N,N*,2,2,6,6-hexamethylpiperidin-4-ammonium-iodide (R-DMAT-7)

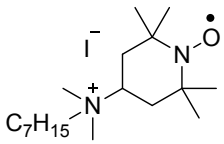

$C_{18}H_{38}IN_2O^{\bullet}$
425.41 g/mol

The title compound was synthesized according to GP3 with 4-dimethylamino-TEMPO (100 mg, 0.502 mmol, 1.0 eq.) and 1-iodoheptane (164 μL, 1.00 mmol, 2.0 eq.) in EtOH (0.70 mL) at 80 °C for 24 h. MPLC afforded the title compound as an orange oil (144 mg, 339 μmol, 67%).

IR (ATR, neat): 2928*s*, 1686*m*, 1466*m*, 1382w, 1200s, 1178s, 1131m, 888w, 719m; **HRMS** (ESI, positive mode): *m/z* = 298.2979 calculated for $[M\text{-}I^-]^+$, found: 298.2991.

N-Octyl-1-oxyl-*N,N*,2,2,6,6-hexamethylpiperidin-4-ammonium-iodide (R-DMAT-8)

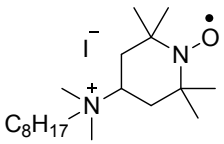

$C_{19}H_{40}IN_2O^{\bullet}$
439.44 g/mol

The title compound was synthesized according to GP3 with 4-dimethylamino-TEMPO (199 mg, 998 μmol, 1.0 eq.) and 1-iodooctane (0.36 mL, 2.0 mmol, 2.0 eq.) in EtOH (1.3 mL) at 80 °C for 24 h. MPLC afforded the title compound as an orange oil (405 mg, 922 μmol, 92%).

IR (ATR): 2926*s*, 2857*m*, 1692*m*, 1464*s*, 1377*m*, 1242*m*, 1180*m*, 892*m*, 674*m*; **HRMS** (ESI, positive mode): *m/z* = 312.3135 calculated for $[M\text{-}I^-]^+$, found: 312.3159.

N-Nonyl-1-oxyl-*N,N*,2,2,6,6-hexamethylpiperidin-4-ammonium-iodide (R-DMAT-9)

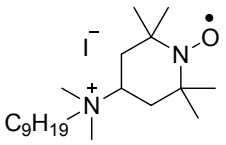

$C_{20}H_{42}IN_2O^{\bullet}$
453.47 g/mol

The title compound was synthesized according to GP3 with 4-dimethylamino-TEMPO (100 mg, 0.502 mmol, 1.0 eq.) and 1-iodononane (198 μL, 1.00 mmol, 2.0 eq.) in EtOH (0.70 mL) at 80 °C for 24 h. MPLC afforded the title compound as an orange solid (97 mg, 214 μmol, 43%).

IR (ATR, neat): 2926s, 1690m, 1466m, 1281w, 1244m, 1201m, 1179m, 719w; **HRMS** (ESI, positive mode): *m/z* = 326.3292 calculated for $[M\text{-}I^-]^+$, found: 326.3292.

N-Decyl-1-oxyl-*N,N*,2,2,6,6-hexamethylpiperidin-4-ammonium-iodide (R-DMAT-10)

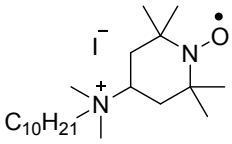

$C_{21}H_{44}IN_2O^{\bullet}$
467.49 g/mol

The title compound was synthesized according to GP3 with 4-dimethylamino-TEMPO (213 mg, 1.07 mmol, 1.0 eq.) and 1-iododecane (456 μL, 2.14 mmol, 2.0 eq.) in EtOH (1.4 mL) at 80 °C for 24 h. MPLC afforded the title compound as an orange solid (319 mg, 682 μmol, 64%).

M.p.: 125 °C; **IR** (ATR, neat): 2923*s*, 2854*m*, 1466*m*, 1366*w*, 1241*m*, 1184*m*, 1101*w*, 893*m*, 722*w*, 671*w*; **HRMS** (ESI, positive mode): *m/z* = 340.4449 calculated for $[M\text{-}I^-]^+$, found: 340.3466.

N-Undecyl-1-oxyl-*N,N*,2,2,6,6-hexamethylpiperidin-4-ammonium-iodide (R-DMAT-11)

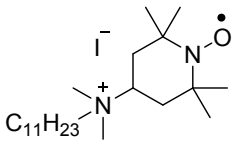

$C_{22}H_{46}IN_2O^{\bullet}$
481.52 g/mol

The title compound was synthesized according to GP3 with 4-dimethylamino-TEMPO (100 mg, 0.502 mmol, 1.0 eq.) and 1-iodoundecane (283 mg, 1.00 mmol, 2.0 eq.) in EtOH (0.7 mL) at 80 °C for 24 h. MPLC afforded the title compound as an orange solid (126 mg, 262 μmol, 52%).

M.p.: 94 °C; **IR** (ATR, neat): 2924s, 2854m, 1688w, 1466m, 1380w, 1243m, 1200m, 1180m, 891w, 719m; **HRMS** (ESI, positive mode): *m/z* = 354.3605 calculated for $[M\text{-}I^-]^+$, found: 354.3609.

N-Dodecyl-1-oxyl-*N,N*,2,2,6,6-hexamethylpiperidin-4-ammonium-iodide (R-DMAT-12)

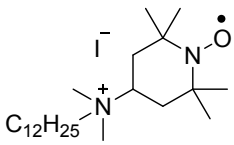

$C_{23}H_{48}IN_2O^{\bullet}$
495.54 g/mol

The title compound was synthesized according to GP3 with 4-dimethylamino-TEMPO (100 mg, 500 μmol, 1.0 eq.) and 1-iododododecane (296 mg, 1.00 mmol, 2.0 eq.) in EtOH (0.70 mL) at 80 °C for 24 h. MPLC afforded the title compound as an orange solid (176 mg, 360 μmol, 71%).

M.p.: 102 °C; **IR** (ATR, neat): 2921*s*, 2853*m*, 1467*m*, 1368*w*, 1241*m*, 1184*m*, 1102*w*, 902*w*, 722*w*; **HRMS** (ESI, positive mode): *m/z* = 368.3762 calculated for $[M\text{-}I^-]^+$, found: 368.3766.

N-Tridecyl-1-oxyl-*N,N,*2,2,6,6-hexamethylpiperidin-4-ammonium-iodide (R-DMAT-13)

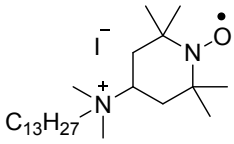

$C_{24}H_{50}IN_2O^{\bullet}$
509.57 g/mol

The title compound was synthesized according to GP3 with 4-dimethylamino-TEMPO (100 mg, 0.502 mmol, 1.0 eq.) and 1-iodotridecane (310 mg, 1.00 mmol, 2.0 eq.) in EtOH (0.70 mL) at 80 °C for 24 h. MPLC afforded the title compound as an orange solid (122 mg, 240 μmol, 48%).

M.p.: 123 °C. **IR** (ATR, neat): 2922*br s*, 2854*m*, 1688*m*, 1466*m*, 1367*m*, 1244*m*, 1181*m*, 888*w*; **HRMS** (ESI, positive mode): *m/z* = 382.3918 calculated for $[M\text{-}I^-]^+$, found: 382.3924.

N-Tetradecyl-1-oxyl-*N,N*,2,2,6,6-hexamethylpiperidin-4-ammonium-iodide (R-DMAT-14)

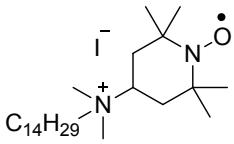

$C_{25}H_{52}IN_2O^{\bullet}$
523.60 g/mol

The title compound was synthesized according to GP3 with 4-dimethylamino-TEMPO (100 mg, 0.502 mmol, 1.0 eq.) and 1-iodotetradecane (324 mg, 1.00 mmol, 2.0 eq.) in EtOH (0.70 mL) at 80 °C for 24 h. MPLC afforded the title compound as an orange solid (193 mg, 370 μmol, 73%).

M.p.: 116 °C; **IR** (ATR, neat): 2923*br s*, 2853*m*, 1626*w*, 1466*m*, 1367*m*, 1260*m*, 1160*m*, 891*w*; **HRMS** (ESI, positive mode): *m/z* = 396.4074 calculated for $[M\text{-}I^-]^+$, found: 396.4098.

N-Pentadecyl-1-oxyl-*N,N*,2,2,6,6-hexamethylpiperidin-4-ammonium-iodide (R-DMAT-15)

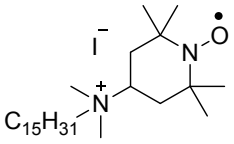

$C_{26}H_{54}IN_2O^{\bullet}$
537.62 g/mol

The title compound was synthesized according to GP3 with 4-dimethylamino-TEMPO (100 mg, 0.502 mmol, 1.0 eq.) and 1-iodopentadecane (338 mg, 1.00 mmol, 2.0 eq.) in EtOH (0.7 mL) at 80 °C for 24 h. MPLC afforded the title compound as an orange solid (197 mg, 370 μmol, 73%).

M.p.: 138 °C; **IR** (ATR, neat): 2923*br s*, 2853*m*, 1651*w*, 1466*m*, 1367*m*, 1261*m*, 1159*m*, 892*w*; **HRMS** (ESI, positive mode): *m/z* = 410.4231 calculated for $[M\text{-}I^-]^+$, found: 410.4264.

N-Hexadecyl-1-oxyl-*N,N*,2,2,6,6-hexamethylpiperidin-4-ammonium-iodide (R-DMAT-16)

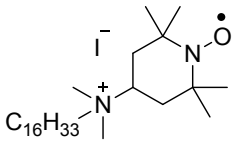

$C_{27}H_{56}IN_2O^{\bullet}$
551.65 g/mol

The title compound was synthesized according to GP3 with 4-dimethylamino-TEMPO (300 mg, 1.51 mmol, 1.0 eq.) and 1-iodohexadecane (583 mg, 1.66 mmol, 1.1 eq.) in EtOH (1.1 mL) at 80 °C for 24 h. MPLC afforded the title compound as an orange solid (328 mg, 595 μmol, 39%).

solubility: not soluble in Et_2O, hardly soluble in EtOAc, good solubility in $CHCl_3$, CH_2Cl_2, CH_3CN, CH_3OH, C_2H_5OH and acetone; **M.p.**: 134 °C; **IR** (ATR, neat): 2918*s*, 2851*m*, 1694*w*, 1470*m*, 1366*w*, 1242*w*, 1183*w*, 1102*w*, 894*w*, 719*w*, 672*w*; **HRMS** (ESI, positive mode): *m/z* = 424.4387 calculated for $[M\text{-}I^-]^+$, found: 424.4394.

N-Heptadecyl-1-oxyl-*N,N*,2,2,6,6-hexamethylpiperidin-4-ammonium-iodide (R-DMAT-17)

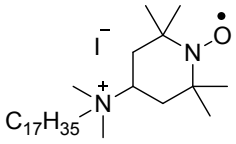

$C_{28}H_{58}IN_2O^{\bullet}$
565.68 g/mol

The title compound was synthesized according to GP3 with 4-dimethylamino-TEMPO (100 mg, 0.502 mmol, 1.0 eq.) and 1-iodoheptadecane (366 mg, 1.00 mmol, 2.0 eq.) in EtOH (0.70 mL) at 80 °C for 24 h. MPLC afforded the title compound as an orange solid (156 mg, 280 μmol, 55%).

M.p.: 118 °C; **IR** (ATR, neat): 2922*br s*, 2853*m*, 1685*w*, 1466*m*, 1367*w*, 1242*m*, 1181*m*, 890*w*; **HRMS** (ESI, positive mode): *m/z* = 438.4544 calculated for $[M\text{-}I^-]^+$, found: 438.4545.

N-Octadecyl-1-oxyl-*N,N*,2,2,6,6-hexamethylpiperidin-4-ammonium-iodide (R-DMAT-18)

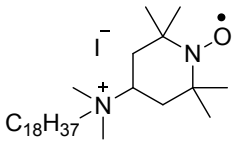

$C_{29}H_{60}IN_2O^{\bullet}$
579.70 g/mol

The title compound was synthesized according to GP3 with 4-dimethylamino-TEMPO (207 mg, 1.04 mmol, 1.0 eq.) and 1-iodoheptadecane (791 mg, 2.08 mmol, 2.0 eq.) in EtOH (1.3 mL) at 80 °C for 24 h. MPLC afforded the title compound as an orange solid (366 mg, 631 μmol, 61%).

M.p.: 128 °C; **IR** (ATR, neat): 2917*s*, 2850*m*, 1470*m*, 1365*w*, 1242*m*, 1183*w*, 904*w*, 718*m*, 671*w*; **HRMS** (ESI, positive mdoe): *m/z* = 452.4701 calculated for $[M\text{-}I^-]^+$, found: 452.4695.

2.5. Synthesis of R-DMAT-16 with Different Counter Anions (X ≠ I):

***N*-Hexadecyl-1-oxyl-*N*,*N*,2,2,6,6-hexamethylpiperidin-4-ammonium-bromide (R-DMAT-16; X = Br)**

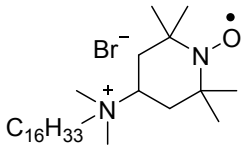

$C_{27}H_{56}BrN_2O^{\bullet}$
504.65 g/mol

The title compound was synthesized according to GP3 with 4-dimethylamino-TEMPO (162 mg, 813 μmol, 1.0 eq.) and 1-bromohexadecane (498 μL, 1.63 mmol, 2.0 eq.) in EtOH (1.1 mL) at 80 °C for 24 h. MPLC afforded the title compound as an orange solid (127 mg, 252 μmol, 31%).

M.p.: 112 °C; **IR** (ATR, neat): 2918*s*, 2851*m*, 1698*w*, 1469*m*, 1364*w*, 1242*m*, 1184*w*, 905*m*, 719*m*; **HRMS** (ESI, positive mode): *m/z* = 424.4387 calculated for $[M\text{-}I^-]^+$, found: 424.4402.

***N*-Hexadecyl-1-oxyl-*N*,*N*,2,2,6,6-hexamethylpiperidin-4-ammonium-triflate (R-DMAT-16; X = OTf)**

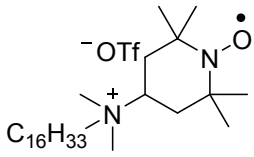

$C_{28}H_{56}F_3N_2O_4S^{\bullet}$
573.82 g/mol

Method I: The title compound was synthesized according to GP3 with 4-dimethylamino-TEMPO (126 mg, 632 μmol, 1.0 eq.) and hexadecyltriflate (473 mg, 1.26 mmol, 2.0 eq.) in EtOAc (1.2 mL) at 80 °C for 24 h. MPLC afforded the title compound as an orange solid (83 mg, 0.15 mmol, 23%).

Method II: The title compound was synthesized according to GP4 with R-DMAT-16 (83 mg, 0.15 mmol, 1.0 eq.) and AgOTf (42 mg, 0.16 mmol, 1.06 eq.) in acetone (5 mL) at rt for 10 min. MPLC afforded the title compound (65 mg, 0.11 mmol, 76%) as an orange solid.

M.p.: 82 °C; **IR** (ATR, neat): 2922*m*, 2853*w*, 1467*w*, 1256*s*, 1155*m*, 1029*m*, 895*w*, 722*w*, 637*m*; **HRMS** (ESI, positive mode): *m/z* = 424.4387 calculated for $[M\text{-}OTf^-]^+$, found: 424.4401, HRMS (ESI, negative mode): *m/z* = 148.9520 calculated for $[OTf]^-$, found: 148.9526.

***N*-Hexadecyl-1-oxyl-*N*,*N*,2,2,6,6-hexamethylpiperidin-4-ammonium-tetrafluoroborate (R-DMAT-16; X = BF_4)**

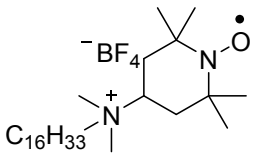

$C_{27}H_{56}BF_4N_2O^{\bullet}$
511.55 g/mol

The title compound was synthesized according to GP4 with R-DMAT-16 (67 mg, 0.12 mmol, 1.0 eq.) and $AgBF_4$ (25 mg, 0.13 mmol, 1.05 eq.) in acetone (5.0 mL) at rt for 10 min. MPLC afforded the title compound (45 mg, 0.09 mmol, 73%) as an orange solid.

M.p.: 93 °C; **IR** (ATR, neat): 2919*s*, 2852*m*, 1470*m*, 1369*w*, 1258*s*, 1155*m*, 1056*s*, 892*w*, 720*w*, 638*m*; **HRMS** (ESI, positive mode): *m/z* = 424.4387 calculated for $[M\text{-}BF_4^-]^+$, found: 424.4401.

***N*-Hexadecyl-1-oxyl-*N*,*N*,2,2,6,6-hexamethylpiperidin-4-ammonium-hexafluorophosphate (R-DMAT-16; X = PF_6)**

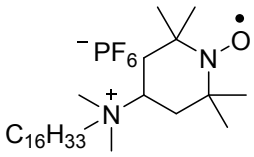

$C_{27}H_{56}F_6N_2OP^{\bullet}$
569.71 g/mol

The title compound was synthesized according to GP4 with R-DMAT-16 (64 mg, 0.12 mmol, 1.0 eq.) and $AgPF_6$ (31 mg, 0.12 mmol, 1.05 eq.) in acetone (5.0 mL) at rt for 10 min. MPLC afforded the title compound (50 mg, 0.09 mmol, 76%) as an orange solid.

M.p.: 79 – 82 °C; **IR** (ATR, neat): 2921*m*, 2852*w*, 1468*w*, 1369*w*, 1242*w*, 1181*w*, 1059*m*, 834*s*, 723*w*, 639*w*; **HRMS** (ESI, positive mode): *m/z* = 424.4387 calculated for $[M\text{-}PF_6^-]^+$, found: 424.4393, **HRMS** (ESI, negative mode): *m/z* = 144.9647 calculated for $[PF_6]^-$, found: 144.9642.

***N*-Hexadecyl-1-oxyl-*N*,*N*,2,2,6,6-hexamethylpiperidin-4-ammonium-hexafluoroantimonate (R-DMAT-16; X = SbF_6)**

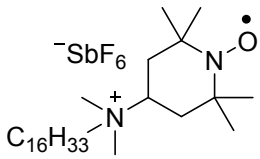

$C_{27}H_{56}F_6N_2OSb^{\bullet}$
660.50 g/mol

The title compound was synthesized according to GP4 with R-DMAT-16 (71 mg, 0.13 mmol, 1.0 eq.) and $AgSbF_6$ (47 mg, 0.14 mmol, 1.05 eq.) in acetone (5.0 mL) at rt for 10 min. MPLC afforded the title compound (43 mg, 0.06 mmol, 50%) as an orange solid.

M.p.: 105 °C; **IR** (ATR, neat): 2923*m*, 2853*w*, 1467*w*, 1369*w*, 1242*w*, 1181*w*, 1058*w*, 835*s*, 722*w*, 659*m*; **HRMS** (ESI, positive mode): *m/z* = 424.4387 calculated for $[M\text{-}SbF_6^-]^+$, found: 424.4401; **HRMS** (ESI, negative mode): *m/z* = 234.8948 calculated for $[SbF_6]^-$, found: 234.8954.

3. Magnetic Characterization

3.1. Magnetic Susceptibility Measurements: Experimental Data and Fits to the Bleaney-Bowers Equation of R-DMAT-n I salts (n = 1 to 18).

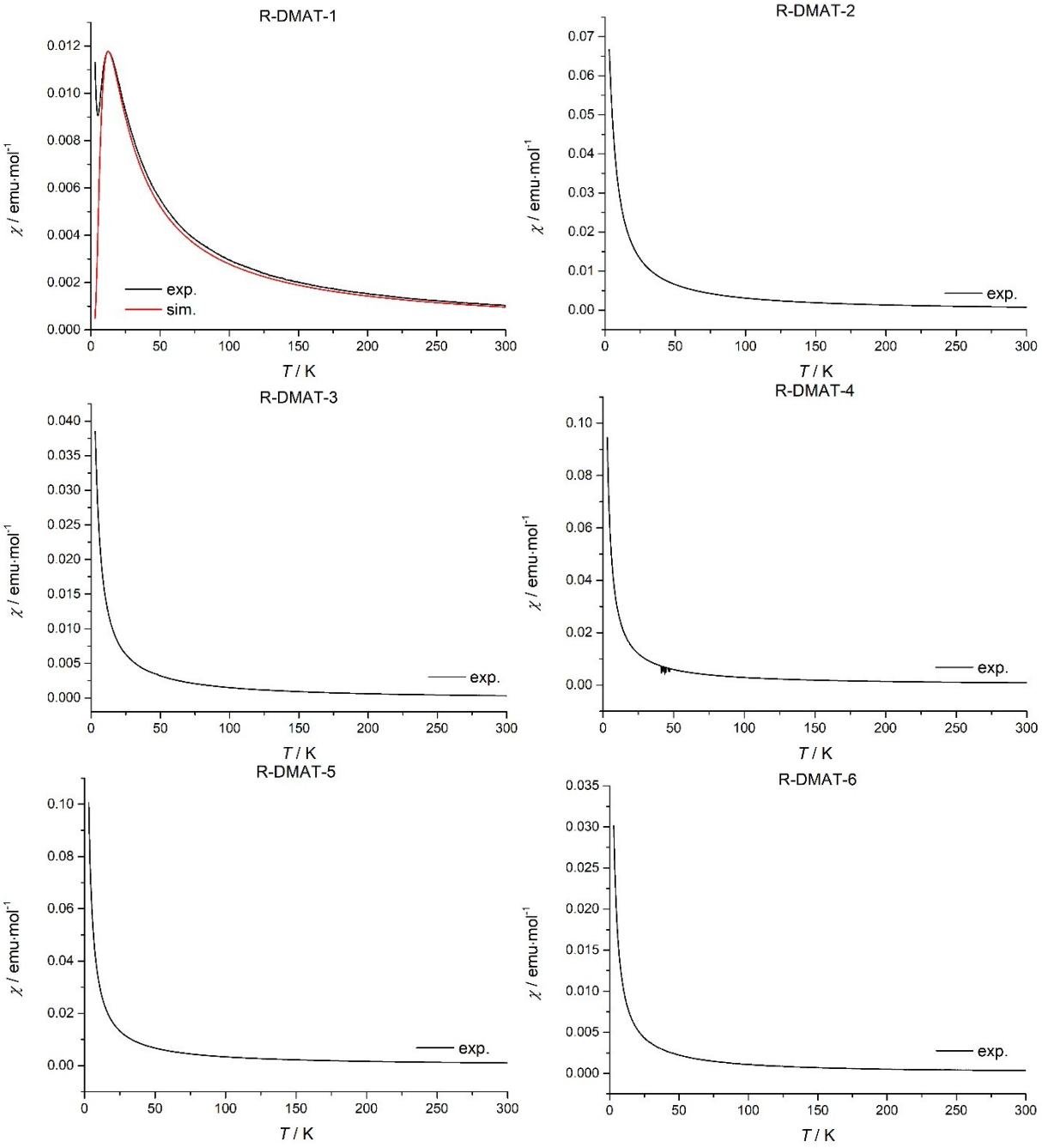

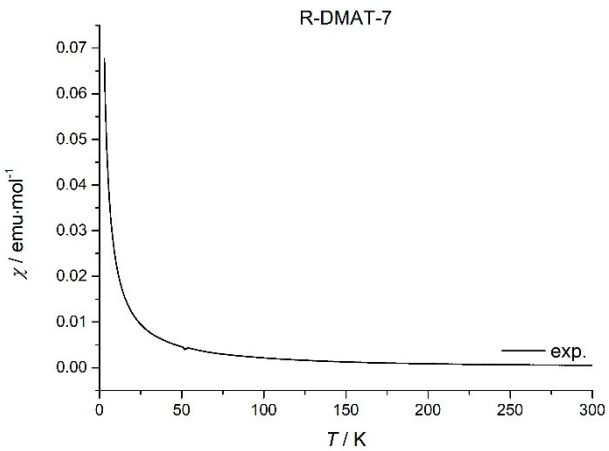
R-DMAT-7
χ / emu·mol⁻¹
T / K
exp.

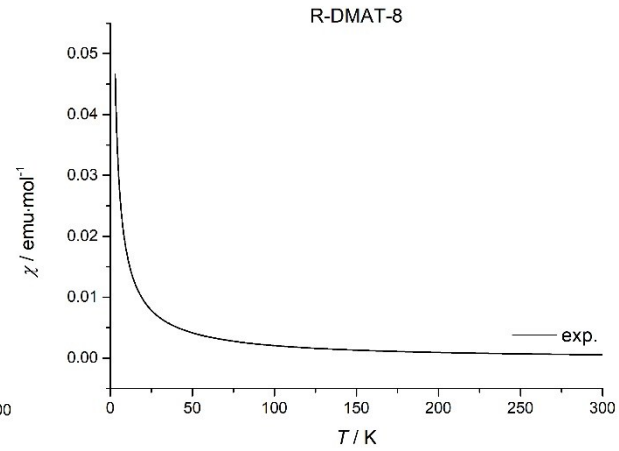
R-DMAT-8
χ / emu·mol⁻¹
T / K
exp.

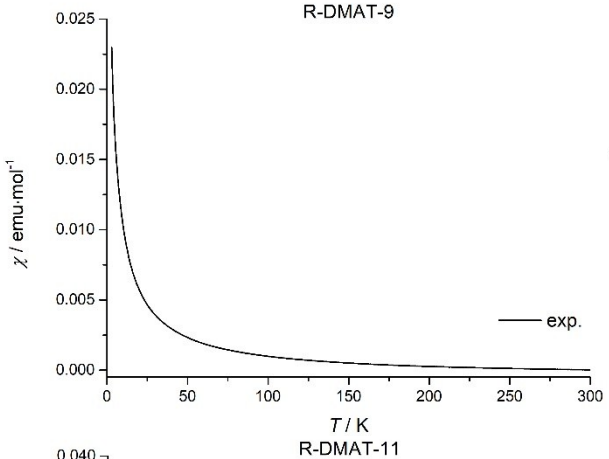
R-DMAT-9
χ / emu·mol⁻¹
T / K
exp.

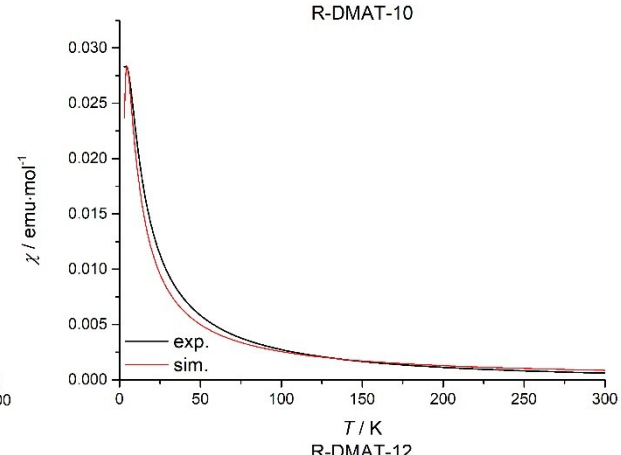
R-DMAT-10
χ / emu·mol⁻¹
T / K
exp.
sim.

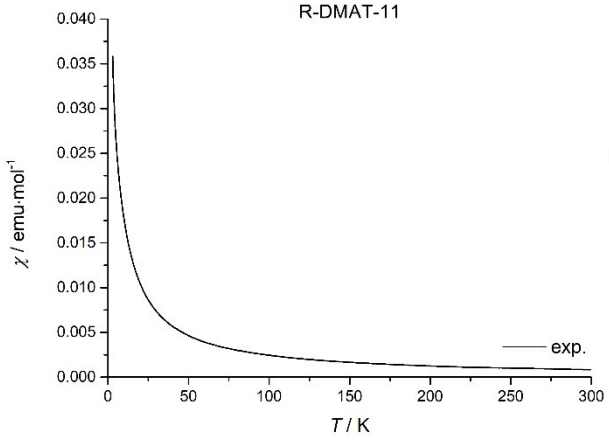
R-DMAT-11
χ / emu·mol⁻¹
T / K
exp.

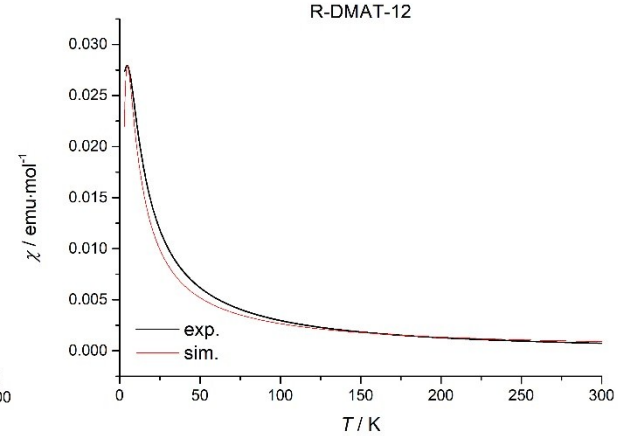
R-DMAT-12
χ / emu·mol⁻¹
T / K
exp.
sim.

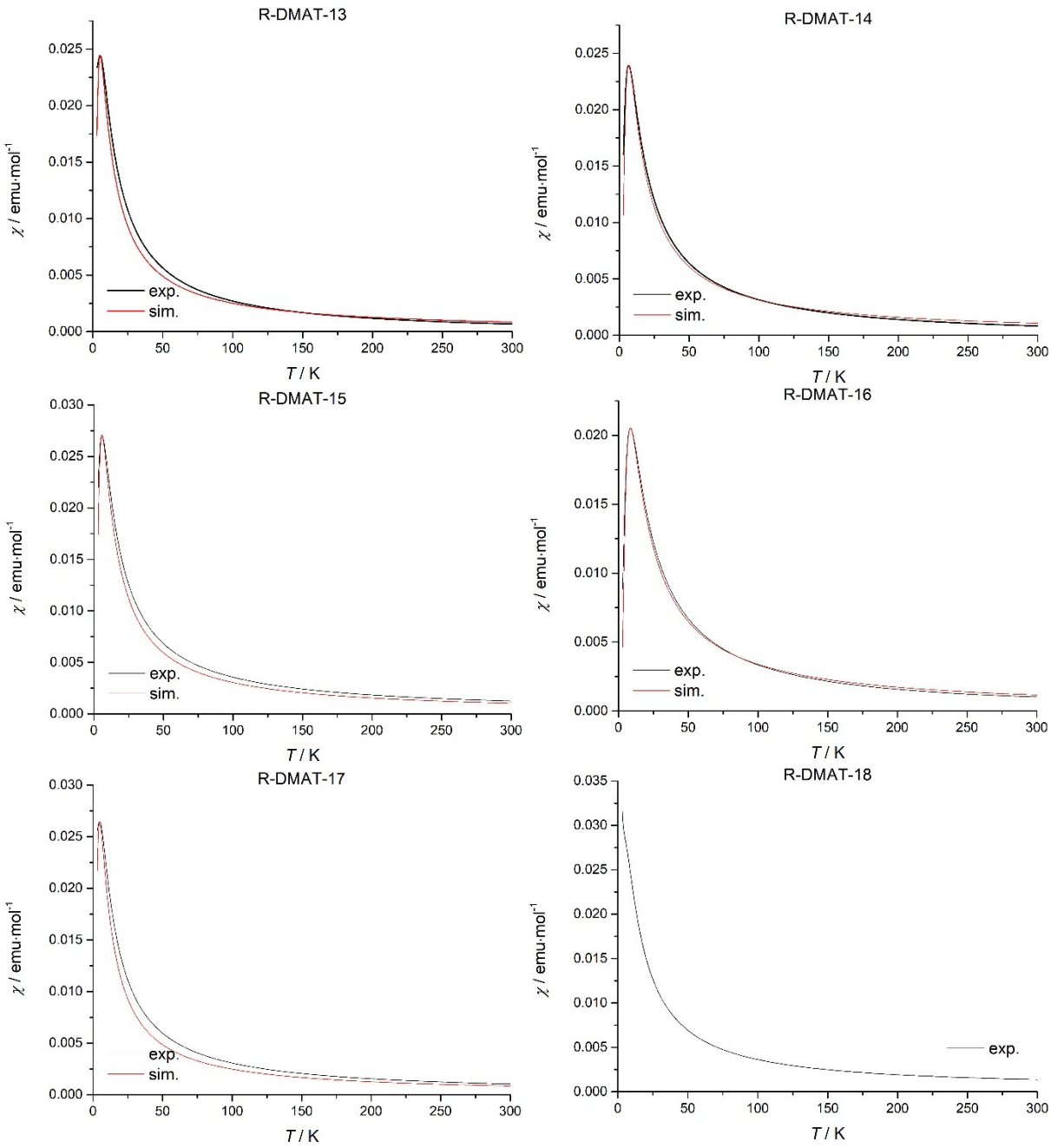

Figure S1: Temperature dependent magnetic susceptibility data as measured by magnetic force detection. Red curves show fits to the Bleaney-Bowers model.

3.2. Temperature Dependent EPR-spectra and Absolute Intensity Measurements of R-DMAT-16 Iodide Triflate Solid Solutions.

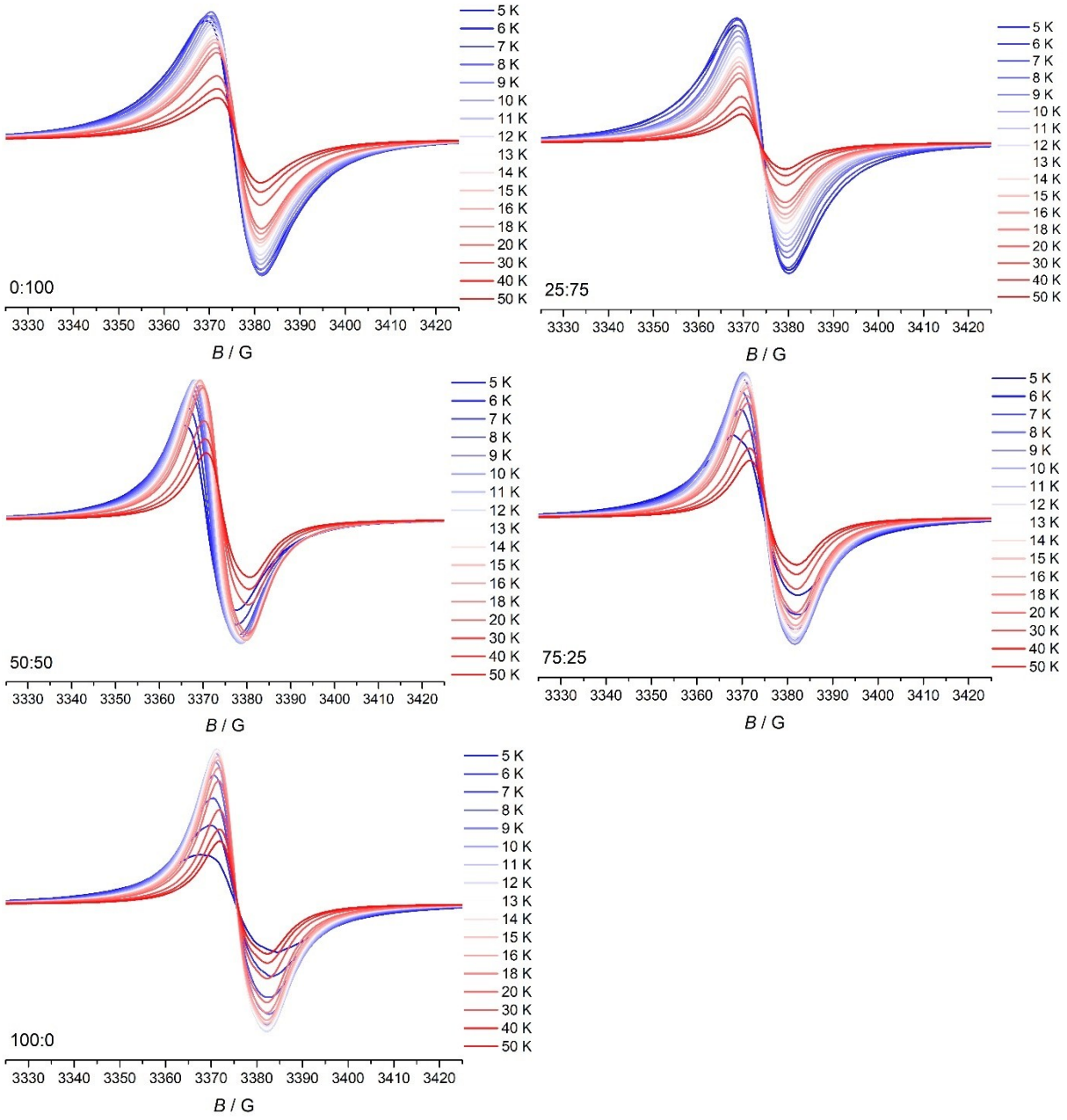

Figure S2: Temperature dependent EPR-spectra and absolute intensity measurements of R-DMAT-16 iodide triflate solid solutions in the range of 5 to 50 K.

3.3. Fits of the Temperature Dependent EPR Signal Intensity Measurements to the Bleaney-Bowers-Equation of R-DMAT-16 Iodide Triflate Solid Solutions.

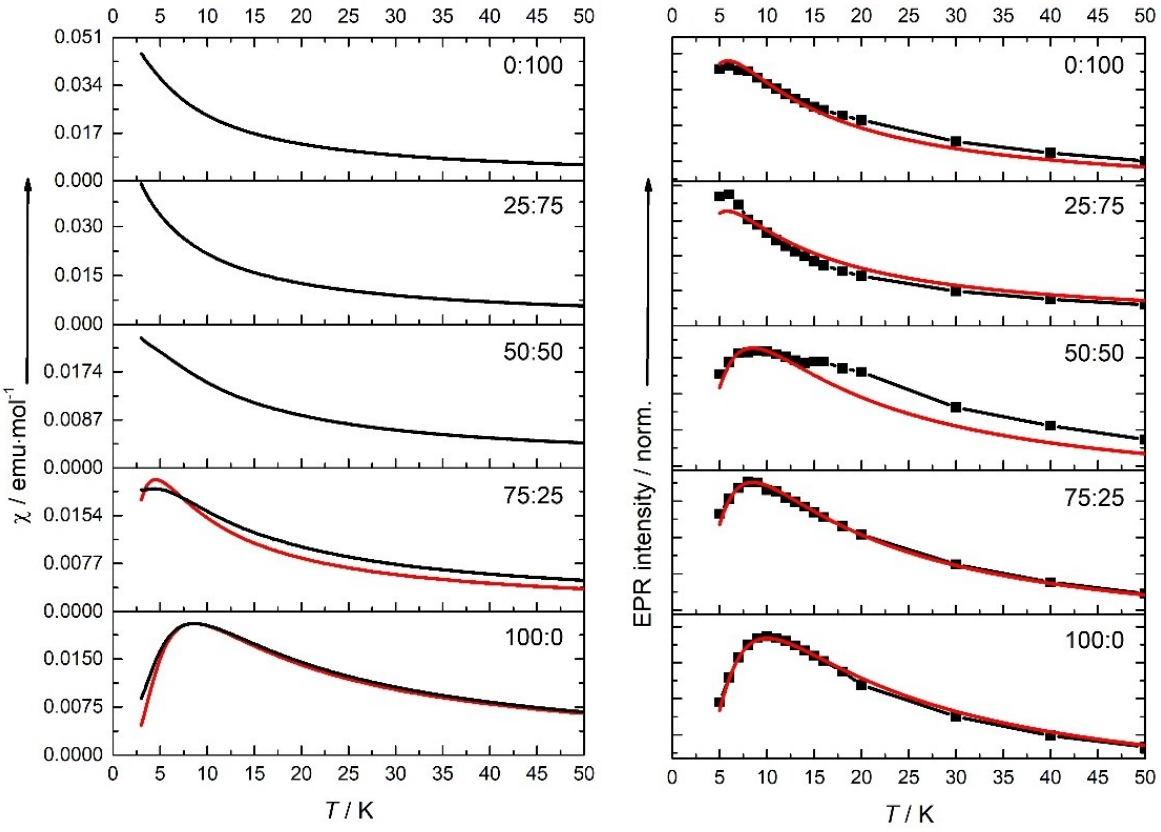

Figure S3: Temperature dependent magnetic susceptibility data as measured by magnetic force detection (left) and (b) by absolute EPR signal quantification (right). The EPR intensities were normalized to the maximum value. Solid curves show fits to the Bleaney-Bowers model.

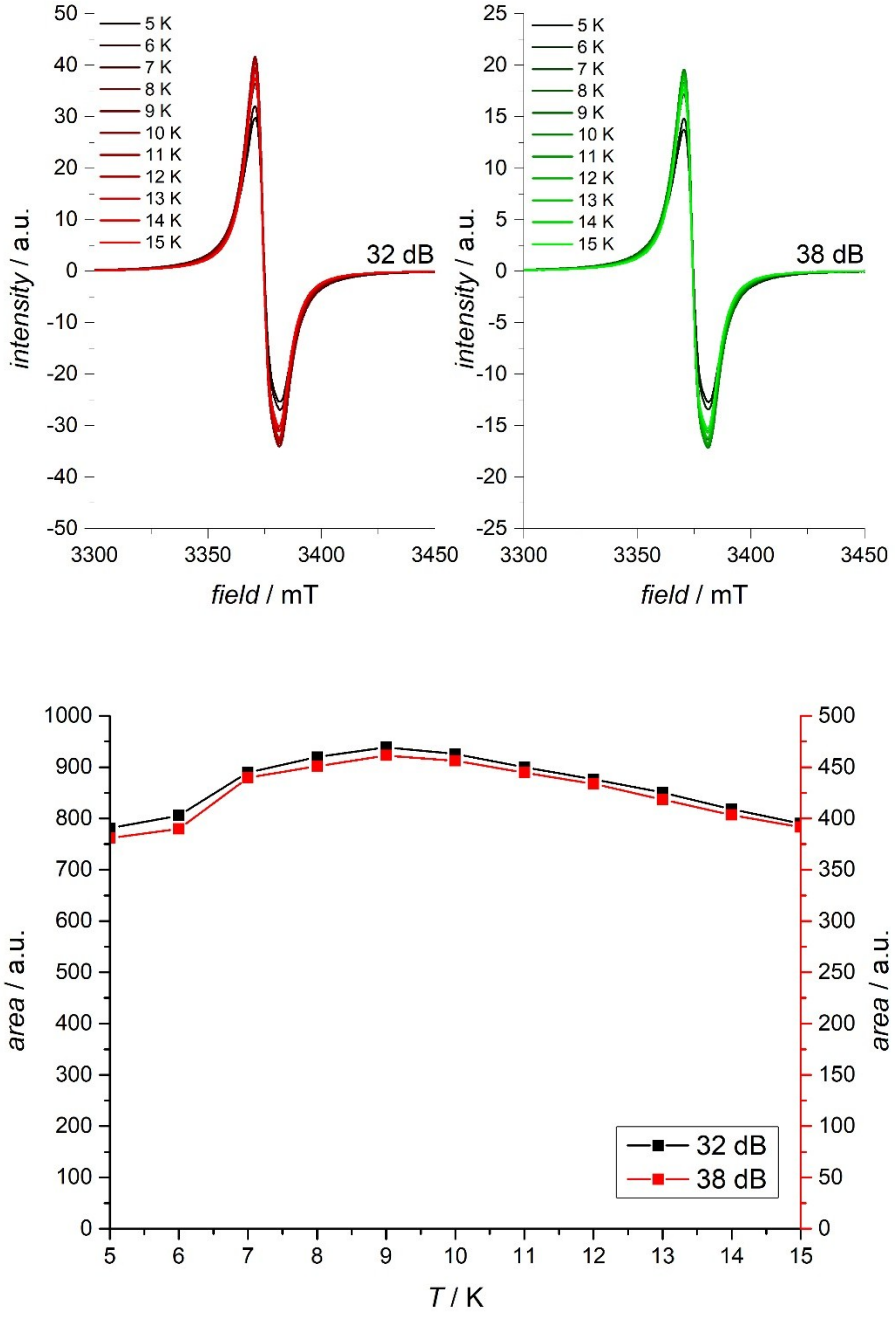

Figure S4: Temperature dependent EPR-spectra and absolute intensity measurements of R-DMAT-16 iodide in the range of 5-15 K: Dependence on the microwave power

Table S1: Curie temperature and coupling constants of various R-DMAT-n Iodides and R-DMAT-16 iodide/triflate mixtures. *measured by cw EPR.

Sample	T_N **/ K**	J **/ cm^{-1}**
R-DMAT-1	12.5	-7.0
R-DMAT-10	4.1	-2.6
R-DMAT-12	4.7	-2.7
R-DMAT-13	5.2	-2.7
R-DMAT-14	6.7	-3.8
R-DMAT-15	5.8	-3.2
R-DMAT-16	8.6	-4.8
R-DMAT-17	4.7	-2.7
R-DMAT-16 (75:25)	4.5	-2.5
* R-DMAT-16 (0:100)	5.8	-3.3
* R-DMAT-16 (25:75)	5.8	-3.3
* R-DMAT-16 (50:50)	8.5	-4.7
* R-DMAT-16 (75:25)	8.5	-4.7
* R-DMAT-16 (100:0)	10.0	-5.6

4. Data Extracted from the Magnetic Force Measurements in R-DMAT-n Iodide Salts and in R-DMAT-16 Salts with Different Counterions.

Table S2: Magnetic properties of R-DMAT-1 to R-DMAT-18 iodides along with the R-DMAT-16 compounds with different anions; μ_{eff}, effective magnetic moment from Curie-Weiss fit, θ_p, paramagnetic Curie temperature, and diamagnetic correction χ_0.

Sample	μ_{eff} / μ_B	θ_p / K	χ_0 (emu mol $^{-1}$)
R-DMAT-1	1.59(1)	–7.0(1)	$-366 \cdot 10^{-6}$
R-DMAT-2	1.64(1)	+2.2(1)	$-387 \cdot 10^{-6}$
R-DMAT-3	1.19(1)	–1.4(1)	$-157 \cdot 10^{-6}$
R-DMAT-4	1.56(1)	–0.1(1)	$-142 \cdot 10^{-6}$
R-DMAT-5	1.70(1)	–2.3(1)	$-408 \cdot 10^{-6}$
R-DMAT-6	0.87(1)	+6.1(1)	$-214 \cdot 10^{-6}$
R-DMAT-7	1.21(1)	+18.2(1)	$-394 \cdot 10^{-6}$
R-DMAT-8	1.37(1)	–3.2(1)	$-510 \cdot 10^{-6}$
R-DMAT-9	1.10(1)	–4.0(1)	$-440 \cdot 10^{-6}$
R-DMAT-10	1.58(1)	+1.0(1)	$-436 \cdot 10^{-6}$
R-DMAT-11	1.44(1)	–5.2(1)	$-339 \cdot 10^{-6}$
R-DMAT-12	1.62(1)	–0.9(1)	$-366 \cdot 10^{-6}$
R-DMAT-13	1.57(1)	–1.0(1)	$-360 \cdot 10^{-6}$
R-DMAT-14	1.70(1)	–2.4(1)	$-372 \cdot 10^{-6}$
R-DMAT-15	1.72(1)	–4.4(1)	$-359 \cdot 10^{-6}$
R-DMAT-16	1.61(1)	+5.2(1)	$-489 \cdot 10^{-6}$
R-DMAT-17	1.58(1)	–2.2(1)	$-417 \cdot 10^{-6}$
R-DMAT-18	1.62(1)	+2.2(1)	$-552 \cdot 10^{-6}$
R-DMAT-16-BF_4	1.58(1)	–2.2(1)	$-524 \cdot 10^{-6}$
R-DMAT-16-Br	1.49(1)	–6.1(1)	$-587 \cdot 10^{-6}$
R-DMAT-16-Cl	1.08(1)	+30.7(1)	$-1092 \cdot 10^{-6}$
R-DMAT-16-OTf	1.54(1)	–2.1(1)	$-609 \cdot 10^{-6}$
R-DMAT-16-PF_6	1.35(1)	–1.9(1)	$-569 \cdot 10^{-6}$
R-DMAT-16-SbF_6	1.26(1)	+0.5(1)	$-444 \cdot 10^{-6}$

5. Magnetic Susceptibility Measurements in R-DMAT-n Iodide Salts and in R-DMAT-16 Salts with Different Counter Ions

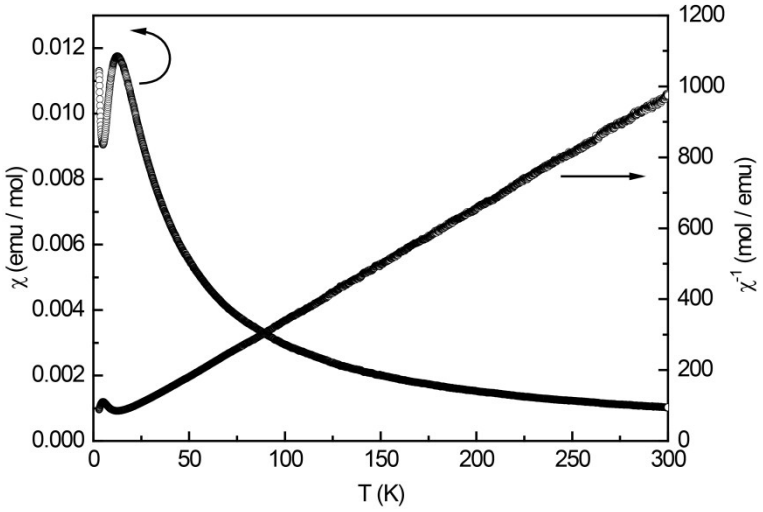

Figure S5: Magnetic properties of **R-DMAT-1**: Temperature dependence of the magnetic susceptibility (χ and χ^{-1} data) measured at 10 kOe.

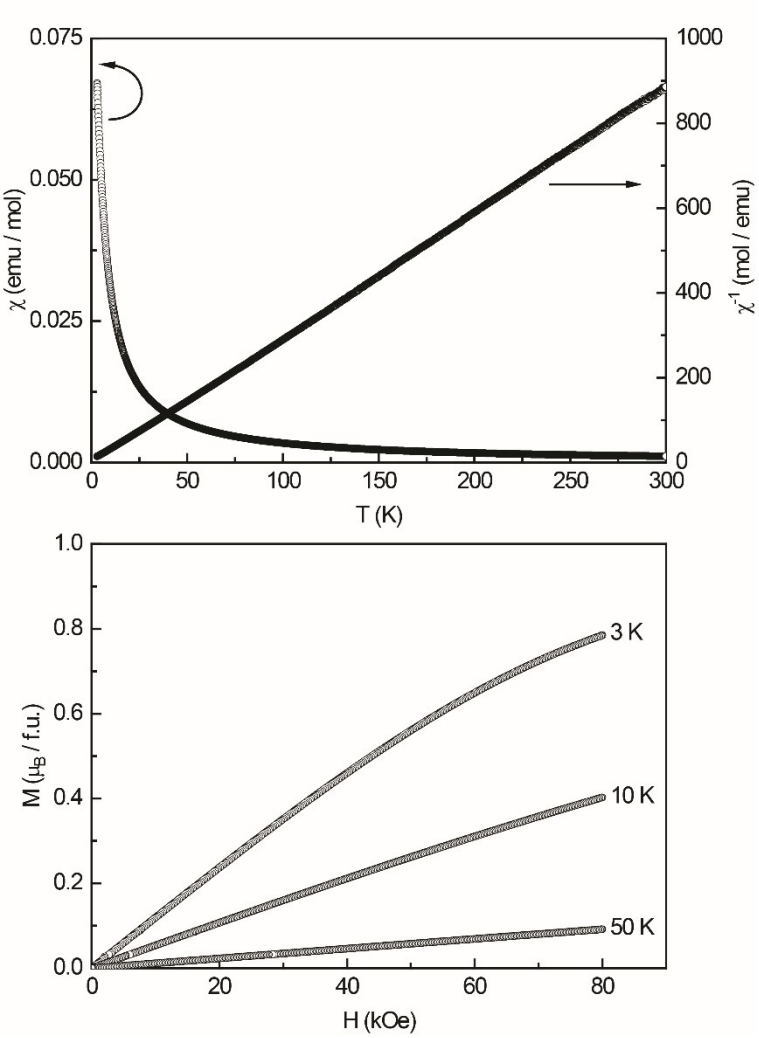

Figure S6: Magnetic properties of **R-DMAT-2**: (top) Temperature dependence of the magnetic susceptibility (χ and χ^{-1} data) measured at 10 kOe; (bottom) Magnetization isotherms recorded at 3, 10 and 50 K.

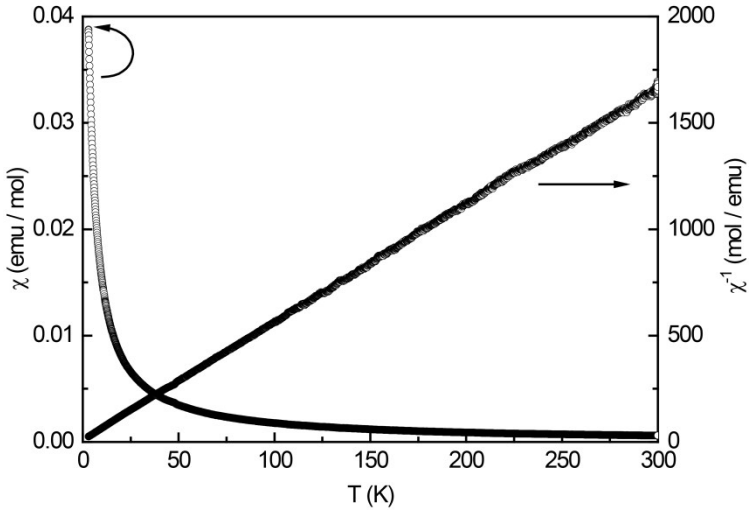

Figure S7: Magnetic properties of **R-DMAT-3**: Temperature dependence of the magnetic susceptibility (χ and χ^{-1} data) measured at 10 kOe.

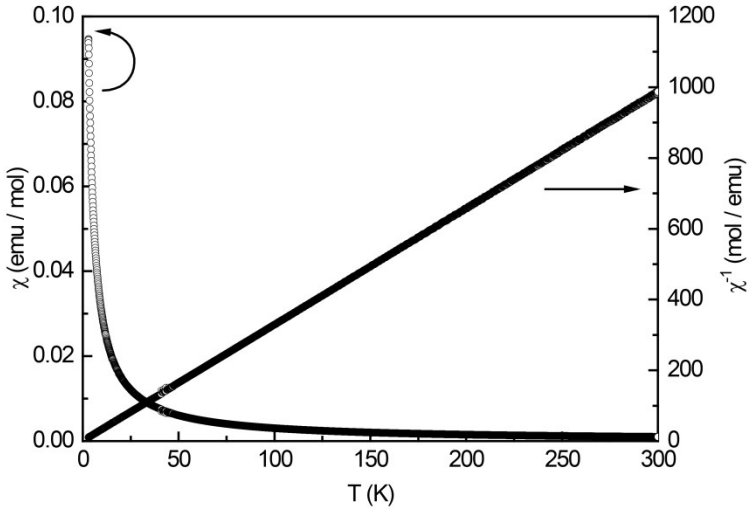

Figure S8: Magnetic properties of **R-DMAT-4**: Temperature dependence of the magnetic susceptibility (χ and χ^{-1} data) measured at 10 kOe.

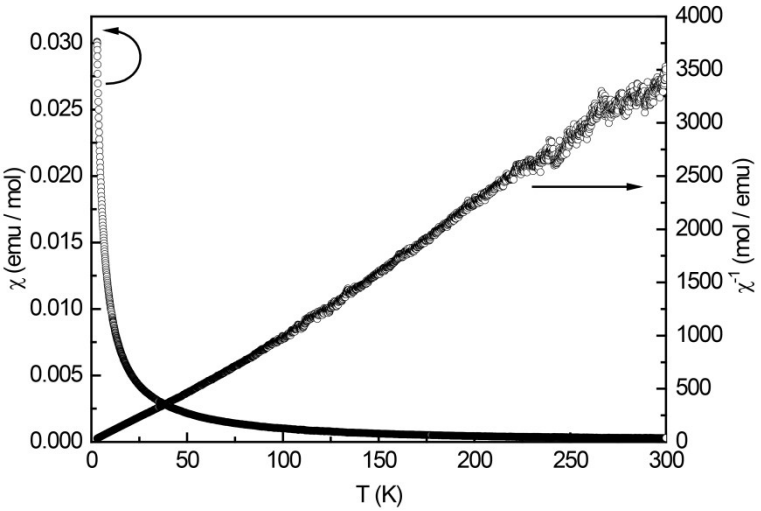

Figure S9: Magnetic properties of **R-DMAT-6**: Temperature dependence of the magnetic susceptibility (χ and χ^{-1} data) measured at 10 kOe.

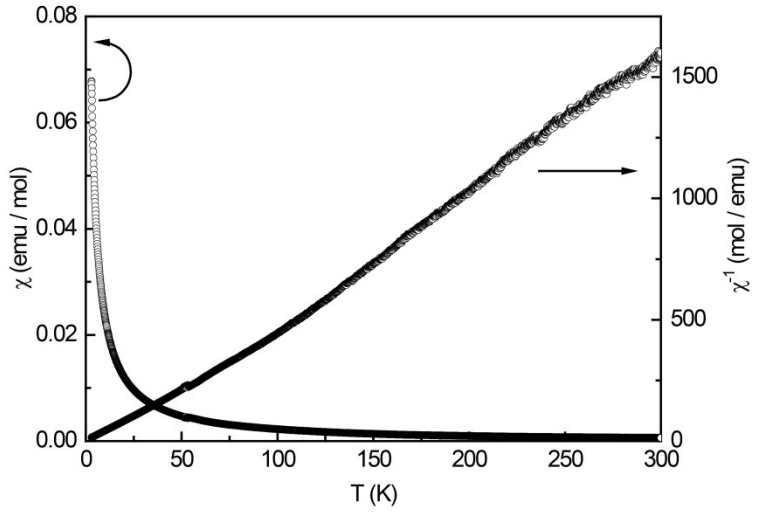

Figure S10: Magnetic properties of **R-DMAT-7**: Temperature dependence of the magnetic susceptibility (χ and χ^{-1} data) measured at 10 kOe.

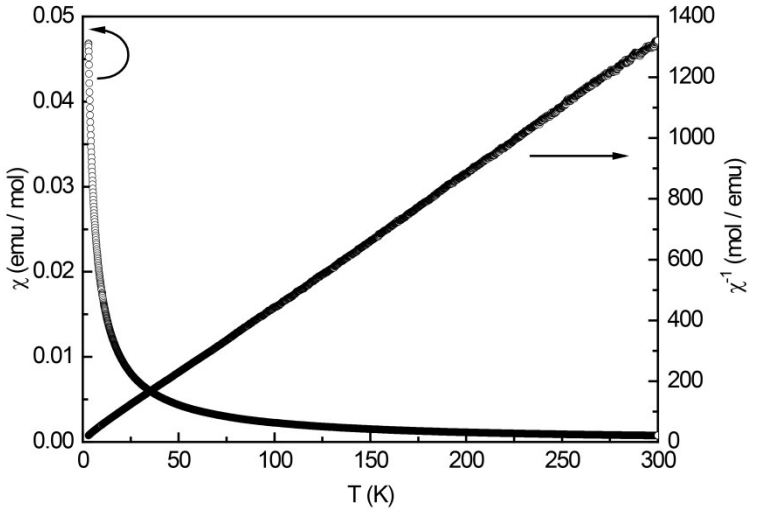

Figure S11: Magnetic properties of **R-DMAT-8**: Temperature dependence of the magnetic susceptibility (χ and χ^{-1} data) measured at 10 kOe.

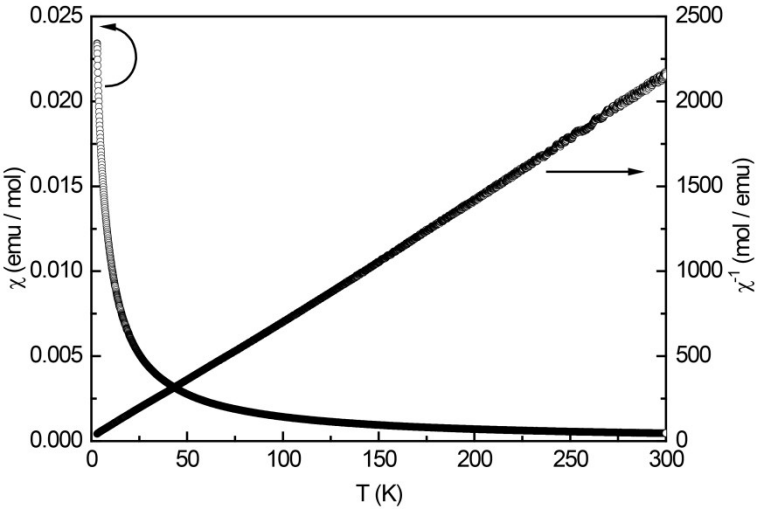

Figure S12: Magnetic properties of **R-DMAT-9**: Temperature dependence of the magnetic susceptibility (χ and χ^{-1} data) measured at 10 kOe.

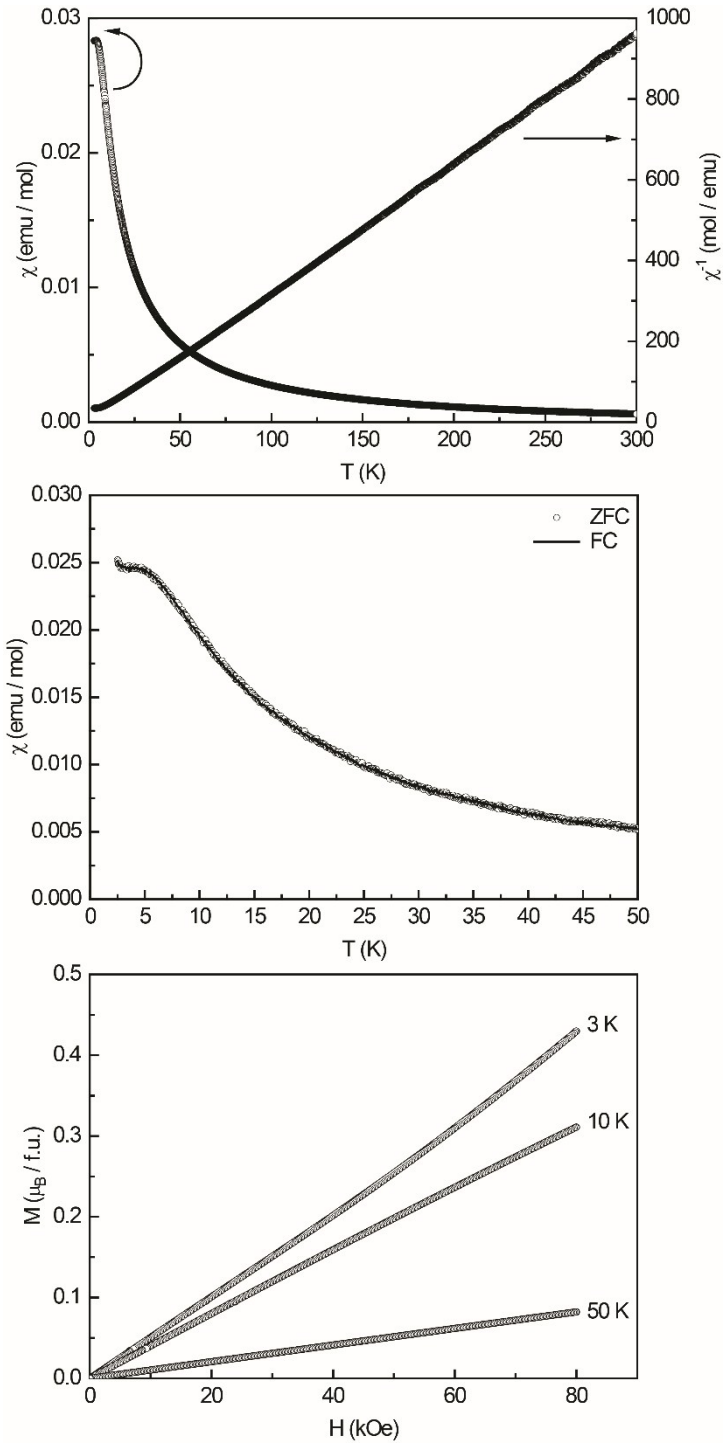

Figure S13: Magnetic properties of **R-DMAT-10**: (top) Temperature dependence of the magnetic susceptibility (χ and χ^{-1} data) measured at 10 kOe; (middle) zero-field-cooled / field-cooled measurements (ZFC/FC); (bottom) Magnetization isotherms recorded at 3, 10 and 50 K.

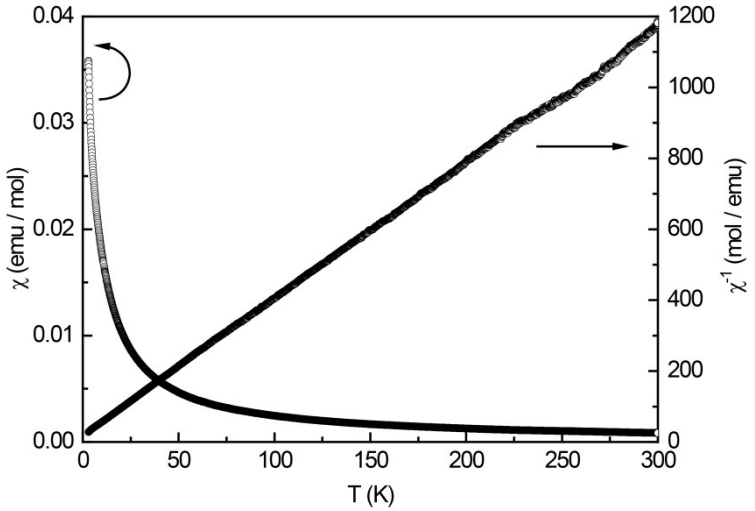

Figure S14: Magnetic properties of **R-DMAT-11**: Temperature dependence of the magnetic susceptibility (χ and χ^{-1} data) measured at 10 kOe.

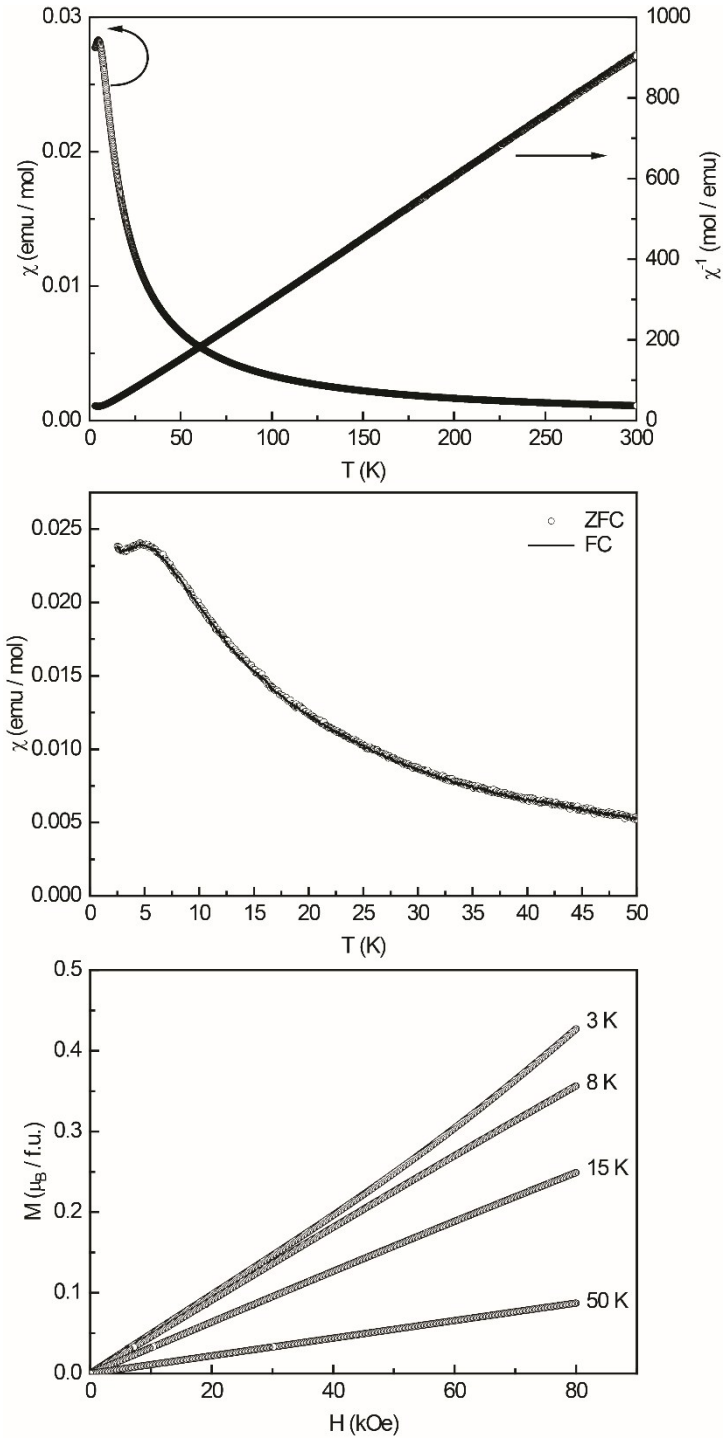

Figure S15: Magnetic properties of **R-DMAT-12**: (top) Temperature dependence of the magnetic susceptibility (χ and χ^{-1} data) measured at 10 kOe; (middle) zero-field-cooled / field-cooled measurements (ZFC/FC); (bottom) Magnetization isotherms recorded at 3, 10 and 50 K.

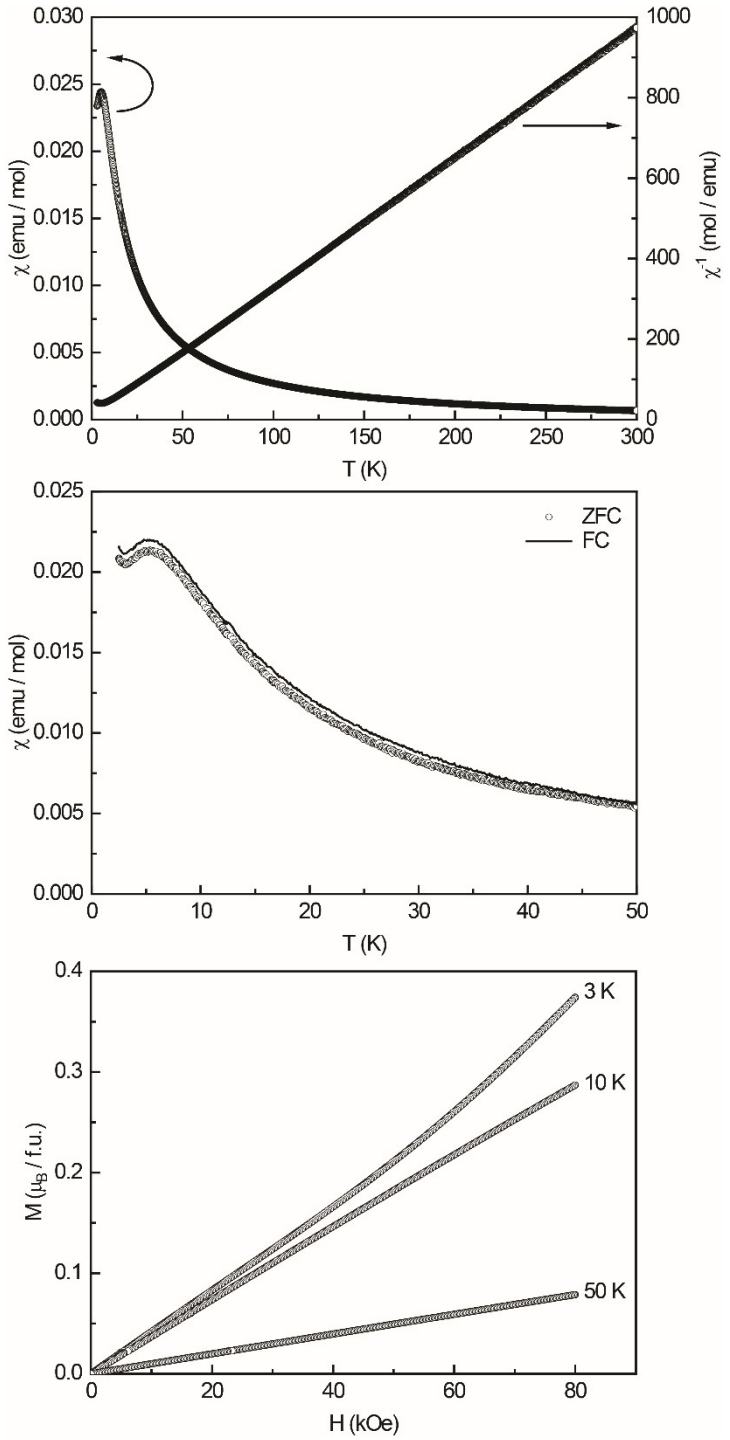

Figure S16: Magnetic properties of **R-DMAT-13**: (top) Temperature dependence of the magnetic susceptibility (χ and χ^{-1} data) measured at 10 kOe; (middle) zero-field-cooled / field-cooled measurements (ZFC/FC); (bottom) Magnetization isotherms recorded at 3, 10 and 50 K.

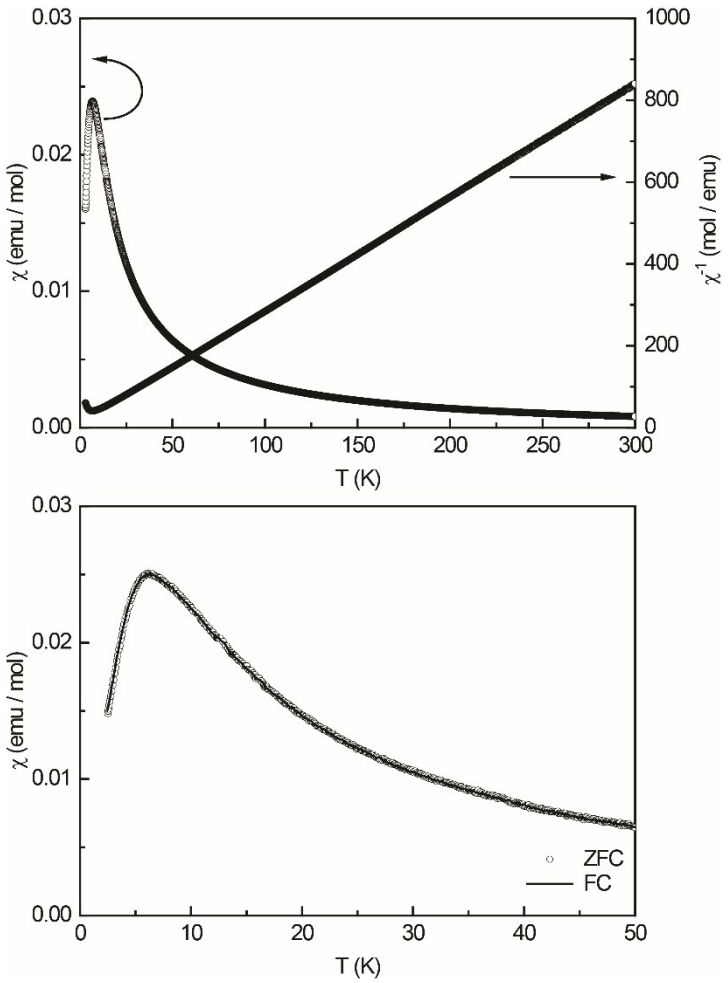

Figure S17: Magnetic properties of **R-DMAT-14**: (top) Temperature dependence of the magnetic susceptibility (χ and χ^{-1} data) measured at 10 kOe; (bottom) zero-field-cooled / field-cooled measurements (ZFC/FC).

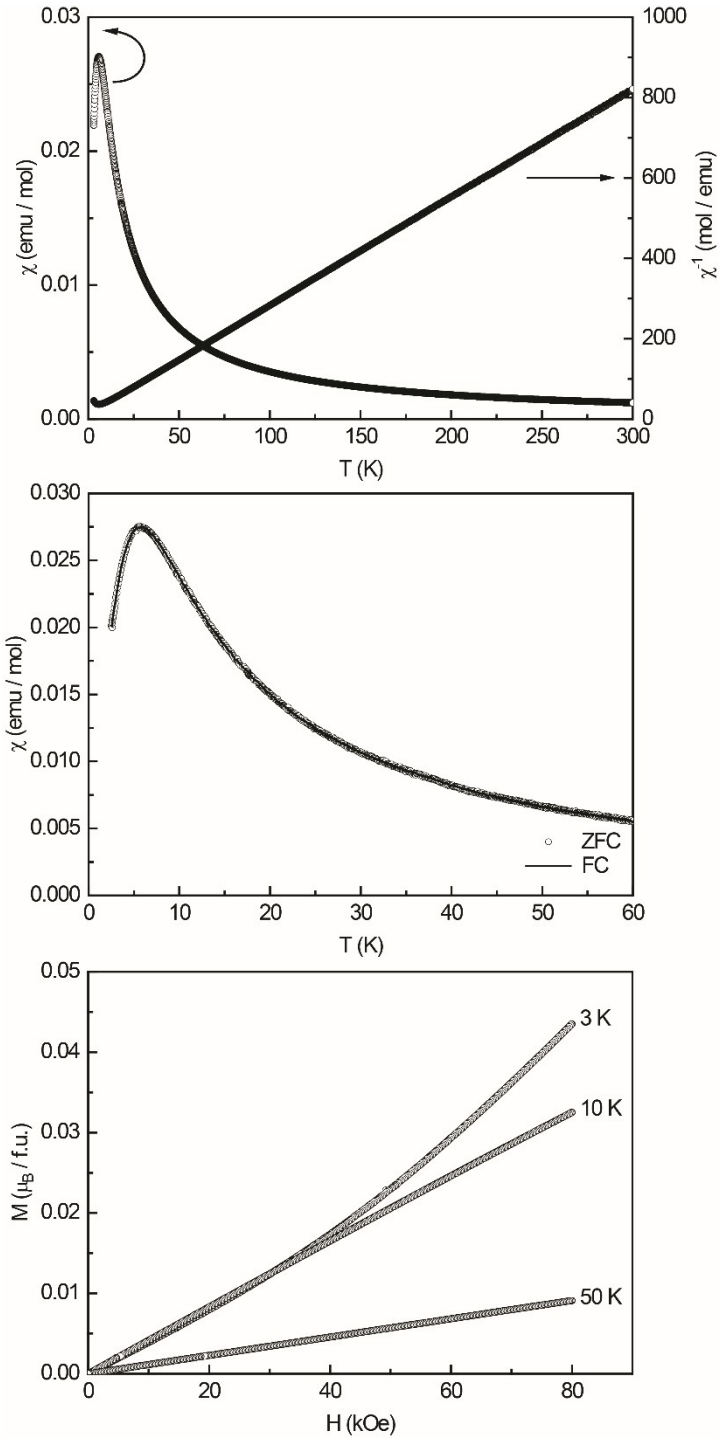

Figure S18: Magnetic properties of **R-DMAT-15**: (top) Temperature dependence of the magnetic susceptibility (χ and χ^{-1} data) measured at 10 kOe; (middle) zero-field-cooled / field-cooled measurements (ZFC/FC); (bottom) Magnetization isotherms recorded at 3, 10 and 50 K.

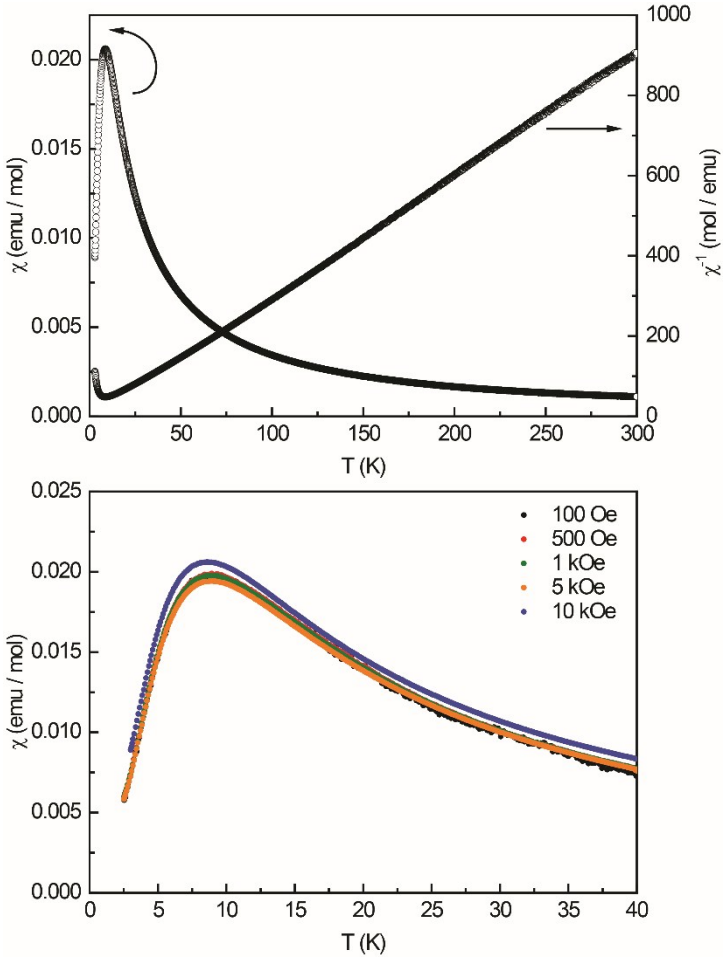

Figure S19: Magnetic properties of **R-DMAT-16**: (top) Temperature dependence of the magnetic susceptibility (χ and χ^{-1} data) measured at 10 kOe; (bottom) field dependent zero-field-cooled measurements.

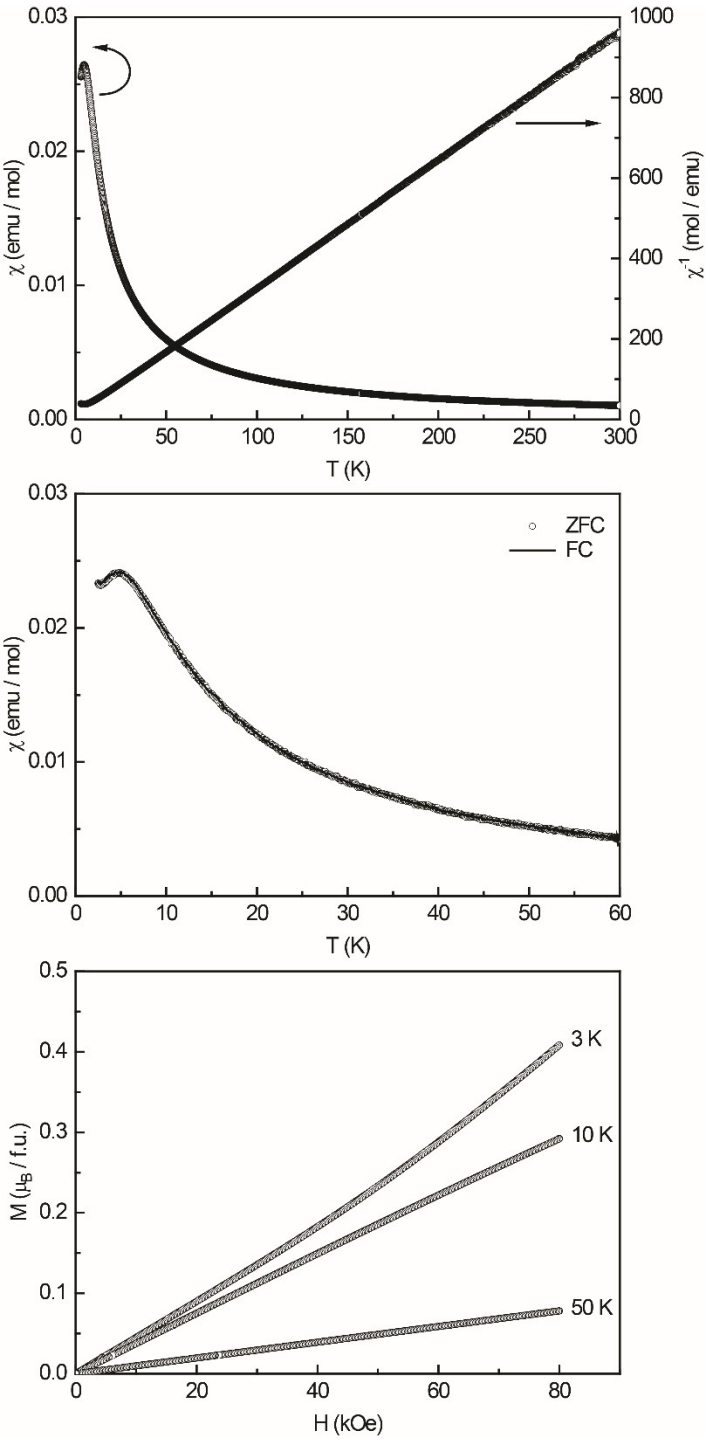

Figure S20: Magnetic properties of **R-DMAT-17**: (top) Temperature dependence of the magnetic susceptibility (χ and χ^{-1} data) measured at 10 kOe; (middle) zero-field-cooled / field-cooled measurements (ZFC/FC); (bottom) Magnetization isotherms recorded at 3, 10 and 50 K.

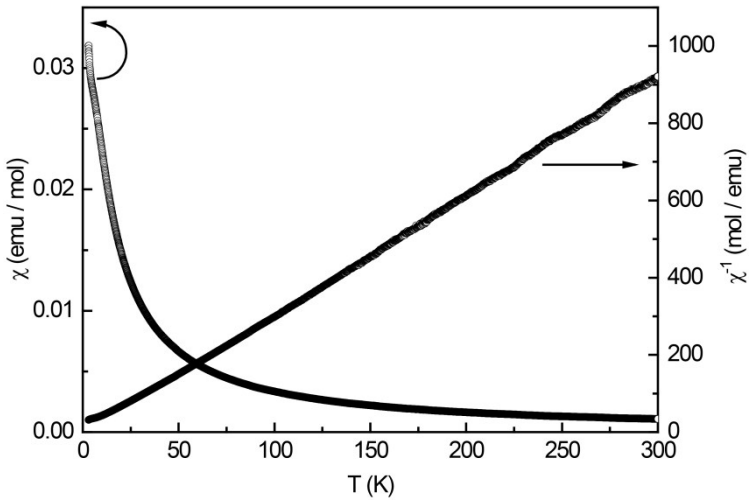

Figure S21: Magnetic properties of **R-DMAT-18**: Temperature dependence of the magnetic susceptibility (χ and χ^{-1} data) measured at 10 kOe.

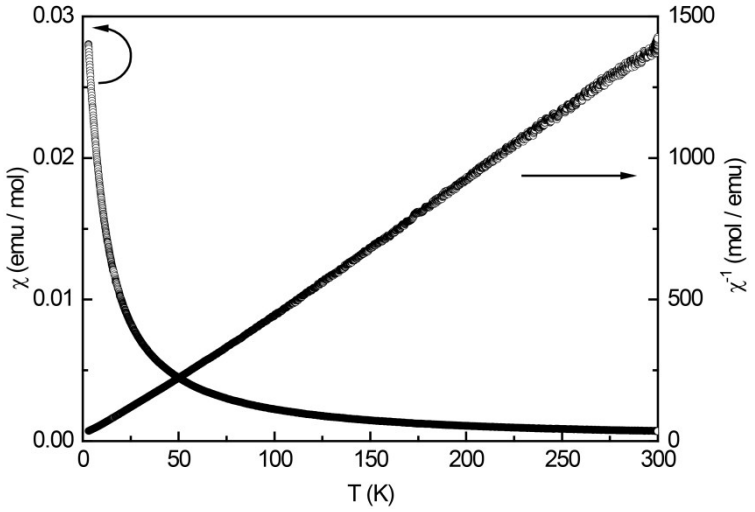

Figure S22: Magnetic properties of **R-DMAT-16-BF_4**: Temperature dependence of the magnetic susceptibility (χ and χ^{-1} data) measured at 10 kOe.

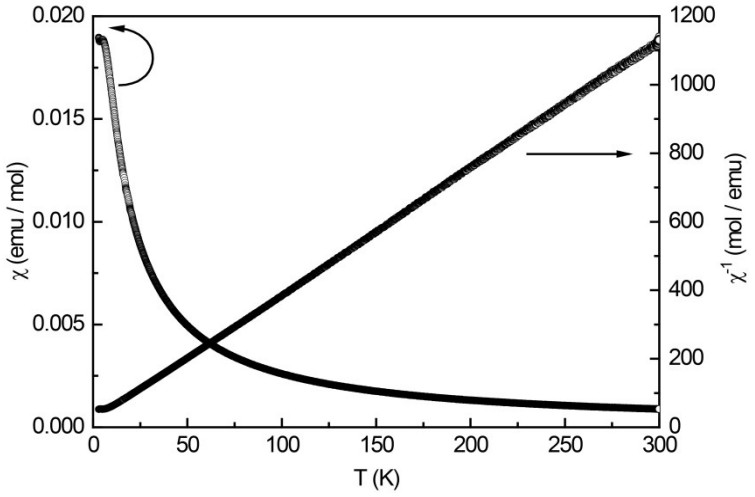

Figure S23: Magnetic properties of **R-DMAT-16-Br**: Temperature dependence of the magnetic susceptibility (χ and χ^{-1} data) measured at 10 kOe.

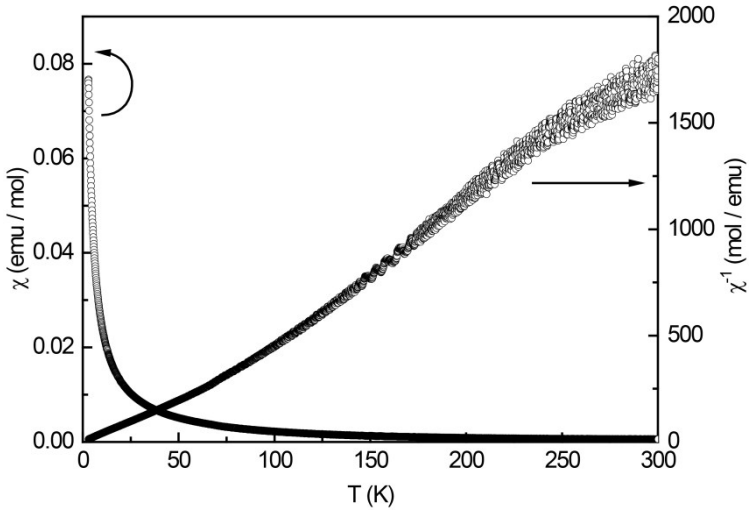

Figure 24: Magnetic properties of **R-DMAT-16-Cl**: Temperature dependence of the magnetic susceptibility (χ and χ^{-1} data) measured at 10 kOe.

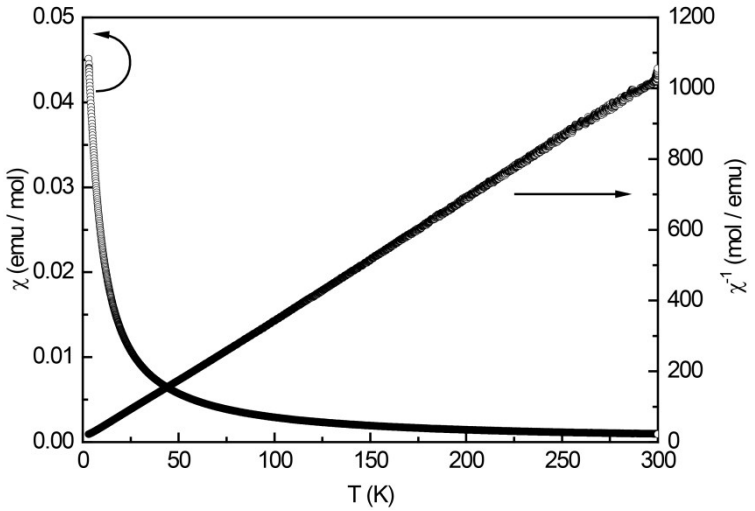

Figure S25: Magnetic properties of **R-DMAT-16-OTf**: Temperature dependence of the magnetic susceptibility (χ and χ^{-1} data) measured at 10 kOe.

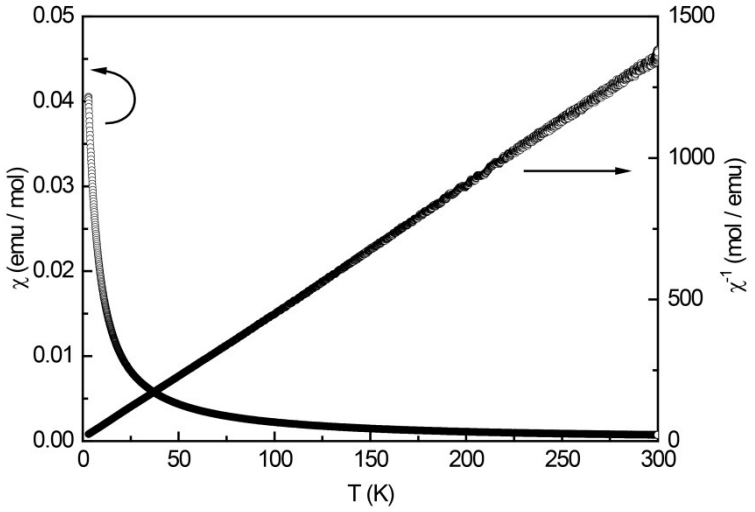

Figure S26: Magnetic properties of **R-DMAT-16-PF_6**: Temperature dependence of the magnetic susceptibility (χ and χ^{-1} data) measured at 10 kOe.

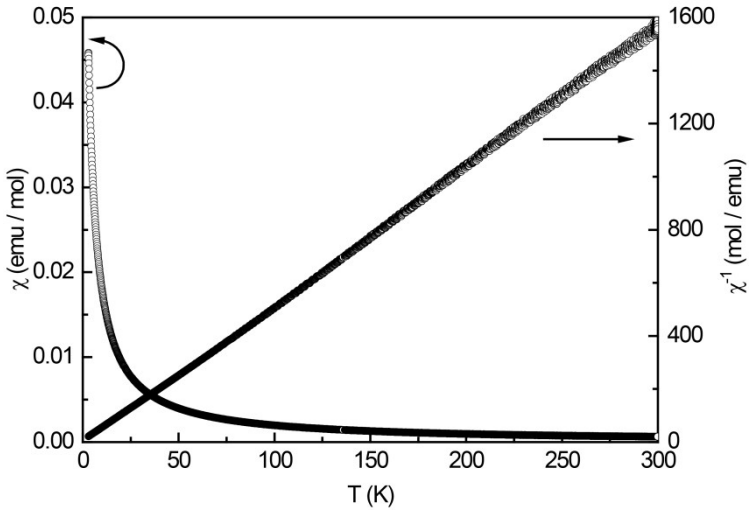

Figure S27: Magnetic properties of **R-DMAT-16-SbF_6**: Temperature dependence of the magnetic susceptibility (χ and χ^{-1} data) measured at 10 kOe.

6. Quantum Chemical Calculations

6.1. Magnetic Susceptibility

Quantum chemical calculations have been performed using the black-box approach described in Ref. [14]. This method is based on the *first-principles bottom-up* approach [15,16] which assumes a Heisenberg Hamiltonian of the form

$$\hat{\mathrm{H}} = -2\sum_{i<j} J_{ij}\hat{\mathrm{S}}_i\hat{\mathrm{S}}_j$$

Here, pairs of local spins ($\hat{S}_i$ and $\hat{S}_j$) on sites *i* and *j* are assumed to interact with each other with a coupling constant J_{ij}. First, all symmetry unique interacting pairs of radical molecules within the crystal structure are identified (the counter ions are neglected). Second, the coupling constant *J* is calculated for each pair with the broken symmetry formalism [17]. These calculations were performed with ORCA 3.0.3 [18] by employing the PBE0 functional [19] and the ma-Def2-TZVP [20] basis set. Third, a minimal magnetic model is created and successively enlarged (for more information see Ref. [14]). The Heisenberg Hamiltonian is set up and diagonalized for each magnetic model. Fourth, the magnetic susceptibility is calculated for each model by assuming a Boltzmann distribution. This allows us to test for convergence of the magnetic model size.

6.1.1. R-DMAT-14 Iodide Salt

Figure S28 depicts the spin topology of R-DMAT-14, resulting from quantum chemical calculations. It shows a zigzag chain with antiferromagnetic couplings (J_2) oriented along the *yz* direction of the crystallographic unit cell. Each molecule in the chain has an additional antiferromagnetic coupling (J_1) in *y* direction of the crystallographic unit cell. The second chain can be obtained from the depicted one by a $\mathrm{X2}$ rotation around the center of the unit cell. Further weak antiferromagnetic interactions (J_3–J_8) connect the two chains present in the unit cell. These interactions were neglected in the representation of the spin topology for clarity. In Table S3, all calculated coupling constants are listed.

Table S3: Calculated magnetic coupling constants for different pair interactions in R-DMAT-14 iodide salt.

J_1 / cm^{-1}	J_2 / cm^{-1}	J_3 / cm^{-1}	J_4 / cm^{-1}	J_5 / cm^{-1}	J_6 / cm^{-1}	J_7 / cm^{-1}	J_8 / cm^{-1}
−1.62	−1.20	−0.19	−0.10	−0.09	−0.08	−0.06	−0.05

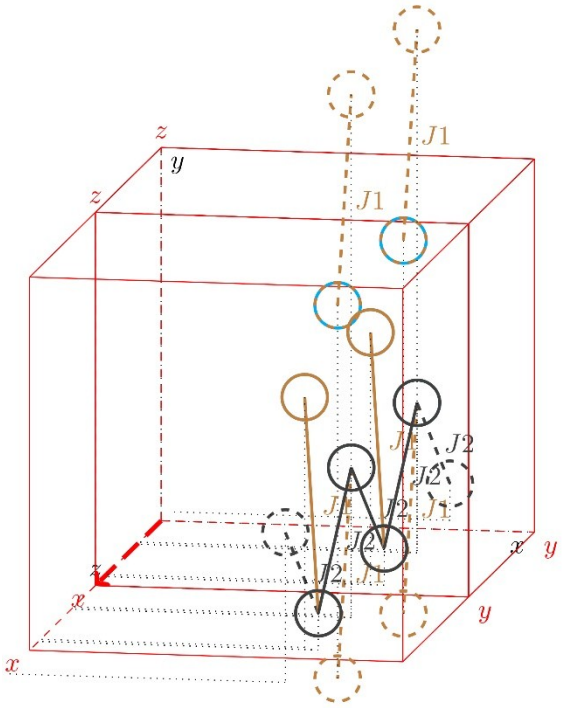

Figure S28: The spin topology of R-DMAT-14 only J_1 and J_2 have been included in this model. Only one from the two identical chains is shown. Each circle represents the center of mass of a molecule. Dashed lines represent magnetic interactions to molecules outside the unit cell. The magnetic cell vectors are shown in red, while the crystallographic cell vectors are shown in black.

The predicted temperature dependent molar magnetic susceptibility curve is shown in Figure S29. Considering only J_1 and J_2, the calculated susceptibility curve shows a transition to the paramagnetic phase at about 2.5 K. Since the unit cell already contains eight molecules, the convergence checks for this system are difficult. Considering only J_1 and J_2 for the magnetic model, the two periodic chains have no interaction with each other. In this case it is sufficient to model two-unit cells in *x* direction of the magnetic unit cell (please note that the Heisenberg Hamiltonian is set up assuming a periodic continuation of that magnetic model). If more coupling constants are included, only a single unit cell can be modelled (due to our chosen settings). It can be seen that a magnetic model which includes more couplings but is modelled with only one-unit cell shows a lower transition temperature.

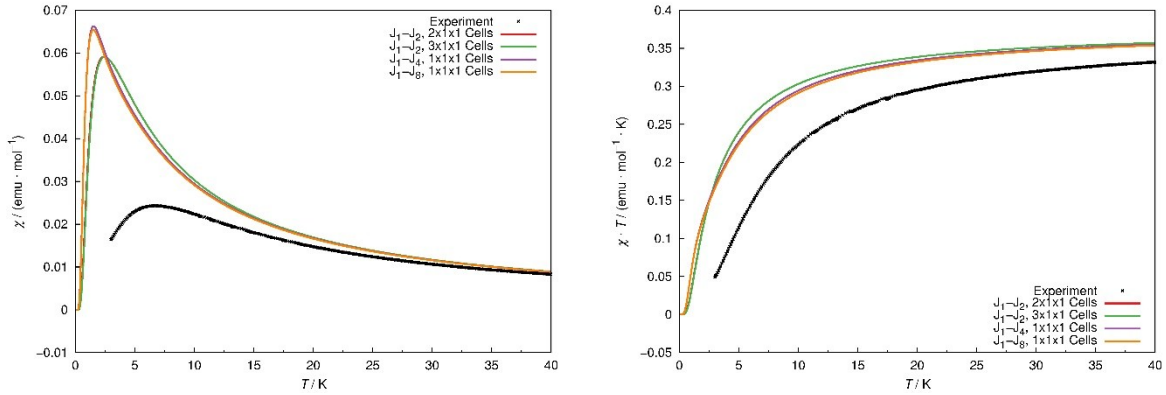

Figure S29: Predicted and measured temperature (T) dependent molar magnetic susceptibility $\chi(T)$ for R-DMAT-14 iodide salt, plotted as $\chi(T)$ versus T (left) and as molar $\chi(T) \cdot T$ versus T (right).

6.1.2. R-DMAT-15 Iodide Salt

The spin topology of R-DMAT-15 is very similar to the one of R-DMAT-14 (see Figure S30 and Figure 28). It can be obtained by a translation of the zigzag chain along the *y* direction of the crystallographic cell. Similar to R-DMAT-14 the second chain can be obtained by a C_2 rotation around the center of the unit cell. The two chains in the unit cell are connected by weak antiferromagnetic interactions (J_3–J_8). The calculated coupling constants are shown in Table S4

Table S4: Calculated magnetic coupling constants for different pair interactions in R-DMAT-15 iodide salt.

J_1 / cm^{-1}	J_2 / cm^{-1}	J_3 / cm^{-1}	J_4 / cm^{-1}	J_5 / cm^{-1}	J_6 / cm^{-1}	J_7 / cm^{-1}	J_8 / cm^{-1}
−1.54	−0.98	−0.50	−0.21	−0.19	−0.12	−0.05	−0.05

The predicted temperature dependent molar magnetic susceptibility curve is depicted in Figure S31. As for R-DMAT-14 the convergence check is difficult. Like for R-DMAT-14 considering only J_1 and J_2 for the magnetic model, it is sufficient to model two-unit cells along the *x* direction of the magnetic unit cell. For this model we observe a transition temperature to the paramagnetic phase of about 2.5 K.

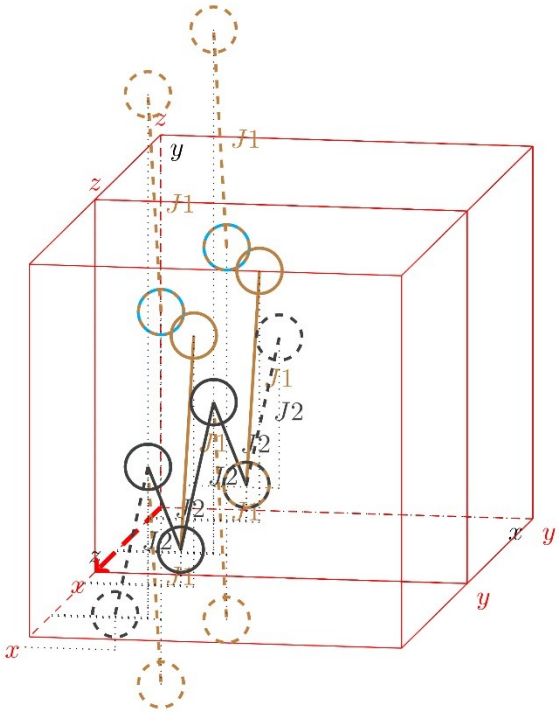

Figure S30: The spin topology of R-DMAT-15; only J_1 and J_2 have been included in this model. Only one of the two identical chains is shown. Each circle represents the center of mass of a molecule. Dashed lines represent magnetic interactions to molecules outside the unit cell. The magnetic cell vectors are shown in red, while the crystallographic cell vectors are shown in black.

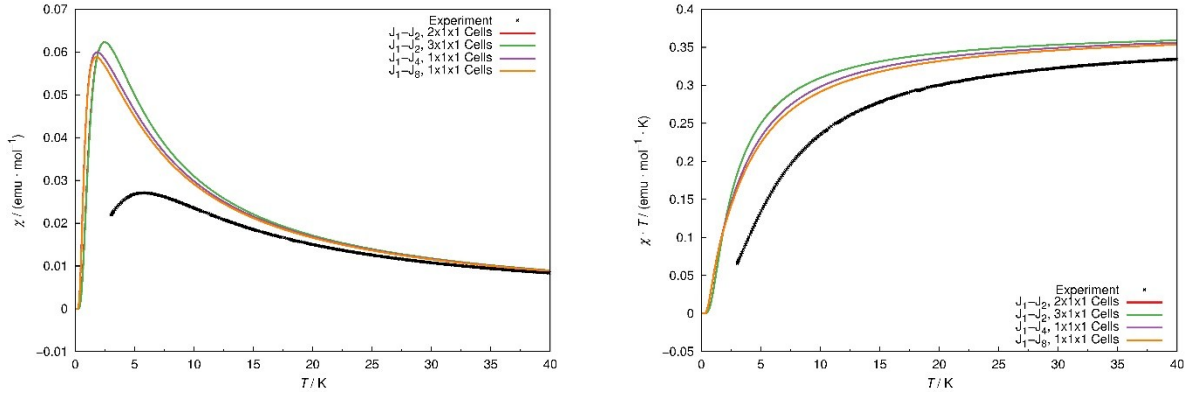

Figure S31: Predicted and measured temperature (T) dependent molar magnetic susceptibility $\chi(T)$ for R-DMAT-15 iodide salt, plotted as χ(T) versus T (left) and as molar $\chi(T) \cdot T$ versus T (right).

6.1.3. R-DMAT-15 Iodide / Triflate (50:50) Salt

The magnetic structure is the same as for the R-DMAT-15 iodide salt (Figure 30). Here, the two chains are connected by a weak ferromagnetic interaction (J_3) and weak antiferromagnetic interactions (J_4 –J_9). The coupling constants are listed in Table S5. The calculated transition temperature to the paramagnetic phase is about 3 K if only J_1 and J_2 are considered for the magnetic model. This model is converged if two-unit cells in the *x* direction of the magnetic unit cell are used. In general, the convergence check for this structure is also difficult (like for R-DMAT-14), but the difference between the different models in the susceptibility plots are smaller. So, the additional couplings between the chains can be neglected.

Table S5: Calculated magnetic coupling constants for different pair interactions in R-DMAT-15 iodide salt.

J_1 / cm^{-1}	J_2 / cm^{-1}	J_3 / cm^{-1}	J_4 / cm^{-1}	J_5 / cm^{-1}	J_6 / cm^{-1}	J_7 / cm^{-1}	J_8 / cm^{-1}	J_9 / cm^{-1}
−1. 91	−1.02	−0.35	−0.18	−0.12	−0.11	−0.05	−0.05	-0.05

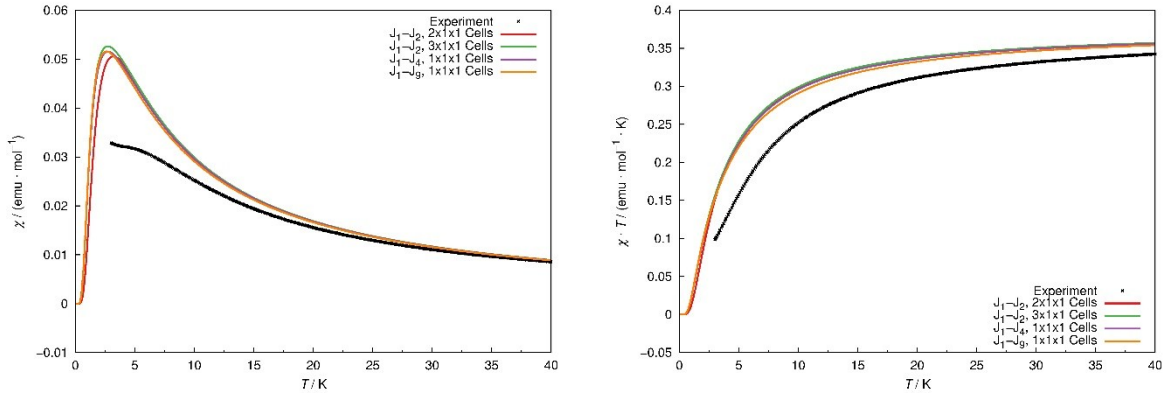

Figure S32: Predicted and measured temperature (T) dependent molar magnetic susceptibility χ(T) for R-DMAT-15 iodide/triflate (50:50) salt, plotted as χ(T) versus T (left) and as molar χ(T) · T versus T (right).

6.1.4. R-DMAT-16 Chloride Salt

The calculated coupling constants for the R-DMAT-16 chloride salt are very weak, see Table S6. Therefore, we refrain from a detailed analysis of the spin topology. Figure S33 depicts the predicted magnetic susceptibility curve. The calculated transition temperature to the paramagnetic phase is about 0.2 K.

Table S6: Calculated magnetic coupling constants for different pair interactions in R-DMAT-16 chloride salt

J_1 / cm^{-1}	J_2 / cm^{-1}	J_3 / cm^{-1}	J_4 / cm^{-1}
−0.08	−0.06	−0.05	−0.05

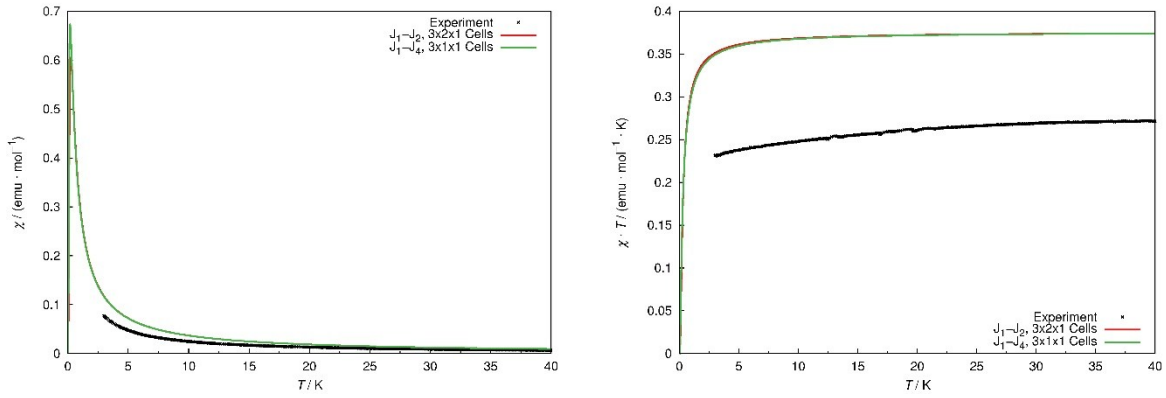

Figure S33: Predicted and measured temperature (T) dependent molar magnetic susceptibility $\chi(T)$ for R-DMAT-16 chloride salt, plotted as $\chi(T)$ versus T (left) and as molar $\chi(T) \cdot$ T versus T (right).

6.2. Dispersion Interaction

To analyze the dependence of the dispersion-interaction strength on the alkyl-chain-length we calculated the D3 dispersion correction [21] with Becke-Johnson [22] damping for various exchange-correlation (XC) functionals for dimers with various alkyl-chain-lengths. This dispersion correction is an additive energy correction to the total energy obtained with a specific XC functional. I.e., its specific value depends on the chosen XC functional. Because of this and because short- and medium range dispersion effects may (at least partially) implicitly be included in the XC approximation, the presented values mainly serve the purpose of highlighting the qualitative behavior of the dispersion interaction.

The dimers were obtained from their respective crystal structures reported here (Section SI-7). For **R-DMAT-1 iodide** we used the crystal structure published by Aonuma *et al* [23]. Table S7 lists the dispersion correction calculated as

$$E^{D3}_{int\ with\ monomer} = E^{D3}_{dimer} - E^{D3}_{monomer\ 1} - E^{D3}_{monomer\ 2}$$

for the dimer with the strongest intermolecular dispersion interaction, extracted from the crystal structure. It is shown that the dispersion correction increases with the alkyl-chain-length from **R-DMAT-1 iodide** to **R-DMAT-15 iodide** for all investigated XC functionals. In case of **R-DMAT-15 iodide / triflate (50:50)** and **R-DMAT-16 chloride** the crystal structure is different which results in a smaller dispersion correction.

Table S7: D3 dispersion correction (in units of kcal) for the strongest interaction of a radical pair extracted from the crystal structure of R-DMAT-X. The dispersion correction was calculated for various XC functionals.

R-DMAT-X iodide:triflate	PBE	BP86	TPSS	B3LYP
R-DMAT-1 100:0	-5	-8	-7	-7
R-DMAT-14 100:0	-13	-20	-16	-18
R-DMAT-15 100:0	-15	-22	-19	-21
R-DMAT-15 50:50	-14	-21	-17	-19
R-DMAT-16 chloride	-10	-15	-12	-13

Furthermore, we investigated the total dispersion interaction (estimated as described above) for a molecule within the crystal structure [24]. We used a supercell with a size of 2x2x4 unit cells and only included the atoms which are within the supercell (the molecules were not completed). The D3 dispersion correction with Becke-Johnson damping and periodic boundary conditions was calculated for the PBE functional. To get the D3 correction for a molecule within the crystal structure we calculated the D3 correction for the whole supercell, for the supercell where one monomer was cut out and for the monomer itself. Afterwards we calculated the D3 correction for the monomer within the crystal structure as

$$E^{D3}_{int\ with\ crystal\ structure} = E^{D3}_{supercell} - E^{D3}_{supercell-monomer} - E^{D3}_{monomer}.$$

Table S8 lists the calculated dispersion corrections for the interaction of a monomer with the environment in the crystal structure for various alkyl-chain-lengths. As for the interaction with a second monomer, the dispersion correction increases with the alkyl-chain-length from **R-DMAT-1 iodide** to **R-DMAT-15 iodide**. As for the pairwise interaction the D3 corrections for **R-DMAT-15 iodide / triflate (50:50)** and **R-DMAT-16 chloride** do not follow the general trend due to a different crystal structure.

Table S8: D3 dispersion correction (in units of kcal) calculated for the interaction of a monomer of R-DMAT-X with the environment in the crystal structure.

R-DMAT-X iodide:triflate	PBE
R-DMAT-1 100:0	-41
R-DMAT-14 100:0	-87
R-DMAT-15 100:0	-94
R-DMAT-15 50:50	-89
R-DMAT-16 chloride	-93

The dispersion interaction between the **R-DMAT-X** monomers is, of course, not solely responsible for the crystal structure, since for example the change of the anion also has an important effect. Nevertheless, the presented results also show that the strength of the dispersion interaction increases with the alkyl-chain-length. Therefore, the significance of the dispersion interaction is higher with longer alkyl-chains.

7. X-ray Crystal Structure Analysis

X-ray crystal structure analysis of R-DMAT-15-I (stu8415): A colorless plate-like specimen of $C_{26}H_{54}IN_2O$, approximate dimensions 0.040 mm x 0.200 mm x 0.200 mm, was used for the X-ray crystallographic analysis. The X-ray intensity data were measured. A total of 1759 frames were collected. The total exposure time was 24.21 h. The frames were integrated with the Bruker SAINT Software package using a wide-frame algorithm. The integration of the data using a monoclinic unit cell yielded a total of 81597 reflections to a maximum θ angle of 66.82° (0.84 Å resolution), of which 10306 were independent (average redundancy 7.917, completeness = 99.2%, R_{int} = 13.98%, R_{sig} = 8.26%) and 7400 (71.80%) were greater than $2\sigma(F^2)$. The final cell constants of *a* = 25.2916(14) Å, *b* = 18.5641(9) Å, *c* = 12.4789(7) Å, *β* = 92.978(4)°, *V* = 5851.1(5) Å^3, are based upon the refinement of the XYZ-centroids of 9137 reflections above 20 σ(I) with 5.908° < 2θ < 128.3°. Data were corrected for absorption effects using the multi-scan method (SADABS). The ratio of minimum to maximum apparent transmission was 0.577. The calculated minimum and maximum transmission coefficients (based on crystal size) are 0.275 and 0.722. The structure was solved and refined using the Bruker SHELXTL Software Package, using the space group $P2_1/c$, with Z = 8 for the formula unit, $C_{26}H_{54}IN_2O$. The final anisotropic full-matrix least-squares refinement on F^2 with 555 variables converged at R1 = 5.85%, for the observed data and wR2 = 15.60% for all data. The goodness-of-fit was 1.041. The largest peak in the final difference electron density synthesis was 0.87 e^-/Å^3 and the largest hole was 1.48 e^-/Å^3 with an RMS deviation of 0.11 e^-/Å^3. On the basis of the final model, the calculated density was 1.22 g/cm^3 and F(000), 2280 e^-. CCDC Nr.: 1826205.

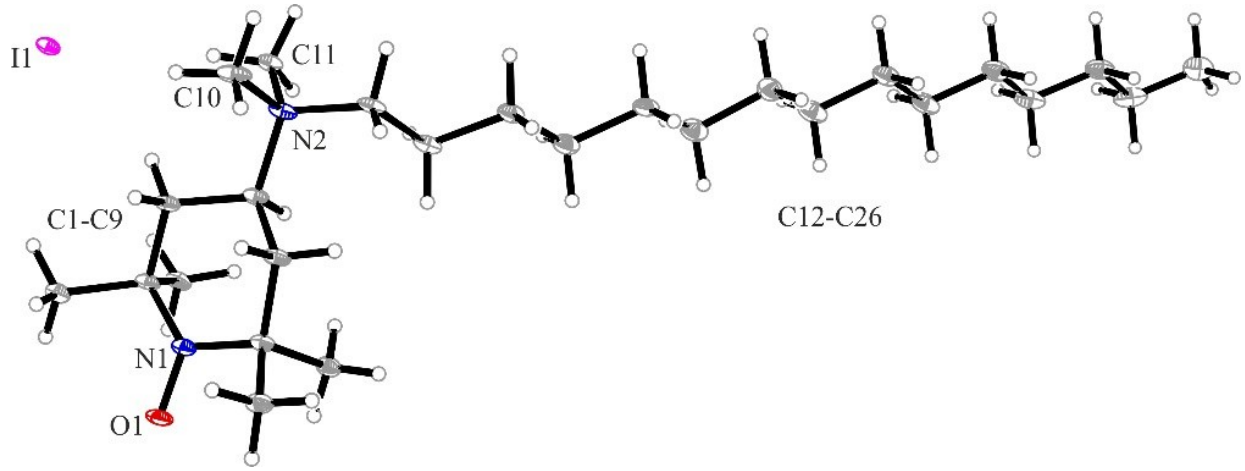

Figure S34: Only one molecule (molecule "A") of two found in the asymmetric unit is shown. Displacement ellipsoids are shown with 15% probability.

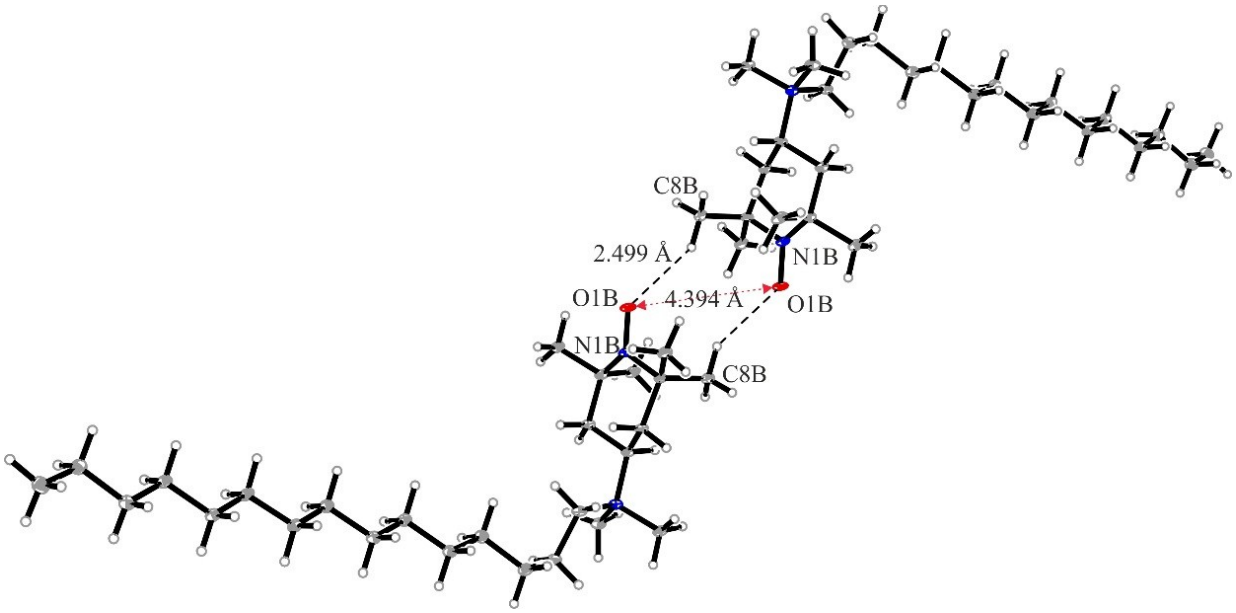

Figure S35: *S*-like shape dimer formation between the molecules "B" involving *C-H···O* hydrogen bonds and the representation of *O1B···O1B* distance 4.394 Å in **R-DMAT-15-I**.

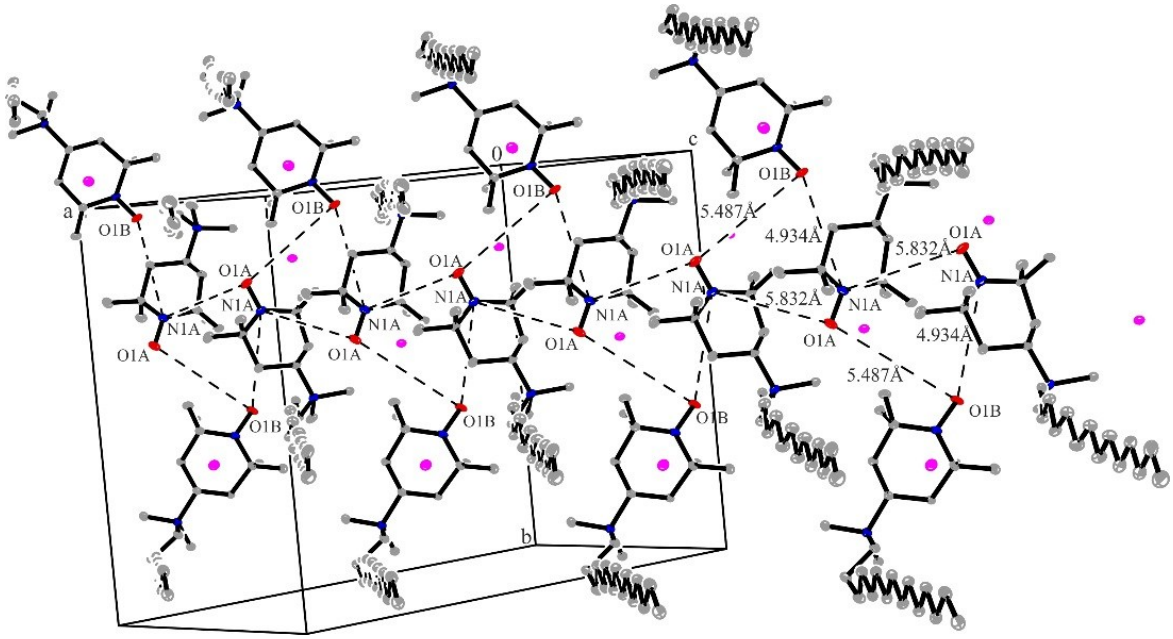

Figure S36: Packing diagram representing the *O···O* and *N···O* interactions along the *c*-axis in **R-DMAT-15-I** (*O1A···O1B* 5.487 Å; *O1A···N1A* 5.832 Å; *O1B···N1A* 4.934 Å).

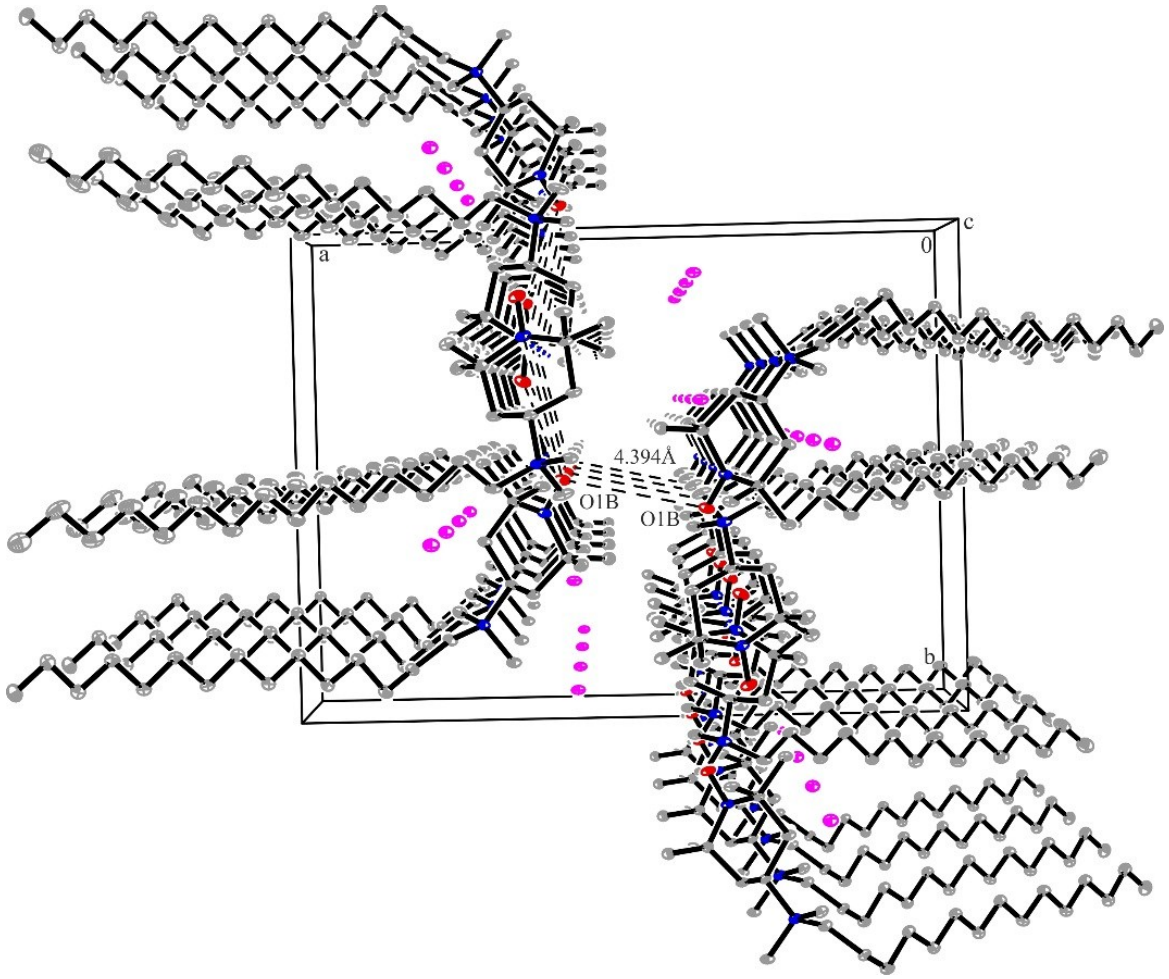

Figure S37: Formation of *S*-like shape between the "B" molecules and the *U*-like shape between the "A" molecules in the packing diagram of **R-DMAT-15-I** (*O⋯O* interactions between the "B" molecules along the *a*-axis: *O1B⋯O1B* 4.394 Å).

7.1. R-DMAT-15 Iodide/Triflate-(45:55 Solid Solution)

X-ray crystal structure analysis of R-DMAT-15-I/OTf (stu8481): A colorless plate-like specimen of $2{\cdot}C_{26}H_{54}N_2O{\cdot}I_{1.45}{\cdot}[CF_3O_3S]_{0.55}$, approximate dimensions 0.070 mm x 0.219 mm x 0.378 mm, was used for the X-ray crystallographic analysis. The X-ray intensity data were measured. The total exposure time was 21.58 h. The frames were integrated with the *Bruker SAINT* Software package using a wide-frame algorithm. The integration of the data using a monoclinic unit cell yielded a total of 72002 reflections to a maximum θ angle of 66.59° (0.84 Å resolution), of which 10496 were independent (average redundancy 6.860, completeness = 99.7%, R_{int} = 8.46%, R_{sig} = 4.93%) and 8895 (84.75%) were greater than $2\sigma(F^2)$. The final cell constants of a = 25.5688(10) Å, b = 18.6362(7) Å, c = 12.5354(5) Å, β = 93.716(2)°, V = 5960.6(4) Å^3, are based upon the refinement of the XYZ-centroids of 9873 reflections above 20 σ(I) with 5.872° < 2θ < 136.7°. Data were corrected for absorption effects using the multi-scan

method (SADABS). The ratio of minimum to maximum apparent transmission was 0.684. The calculated minimum and maximum transmission coefficients (based on crystal size) are 0.189 and 0.654. The structure was solved and refined at using the Bruker SHELXTL Software Package, using the space group $P2_1/c$, with Z = 4 for the formula unit, $2{\cdot}C_{26}H_{54}N_2O{\cdot}I_{1.45}{\cdot}[CF_3O_3S]_{0.55}$. The final anisotropic full-matrix least-squares refinement on F^2 with 628 variables converged at R1 = 5.17%, for the observed data and wR2 = 11.17% for all data. The goodness-of-fit was 1.087. The largest peak in the final difference electron density synthesis was 1.03 $e^-/Å^3$ and the largest hole was 0.56 $e^-/Å^3$ with an RMS deviation of 0.07 $e^-/Å^3$. On the basis of the final model, the calculated density was 1.21 g/cm^3 and F(000), 2324 e^-. CCDC Nr.: 1826206.

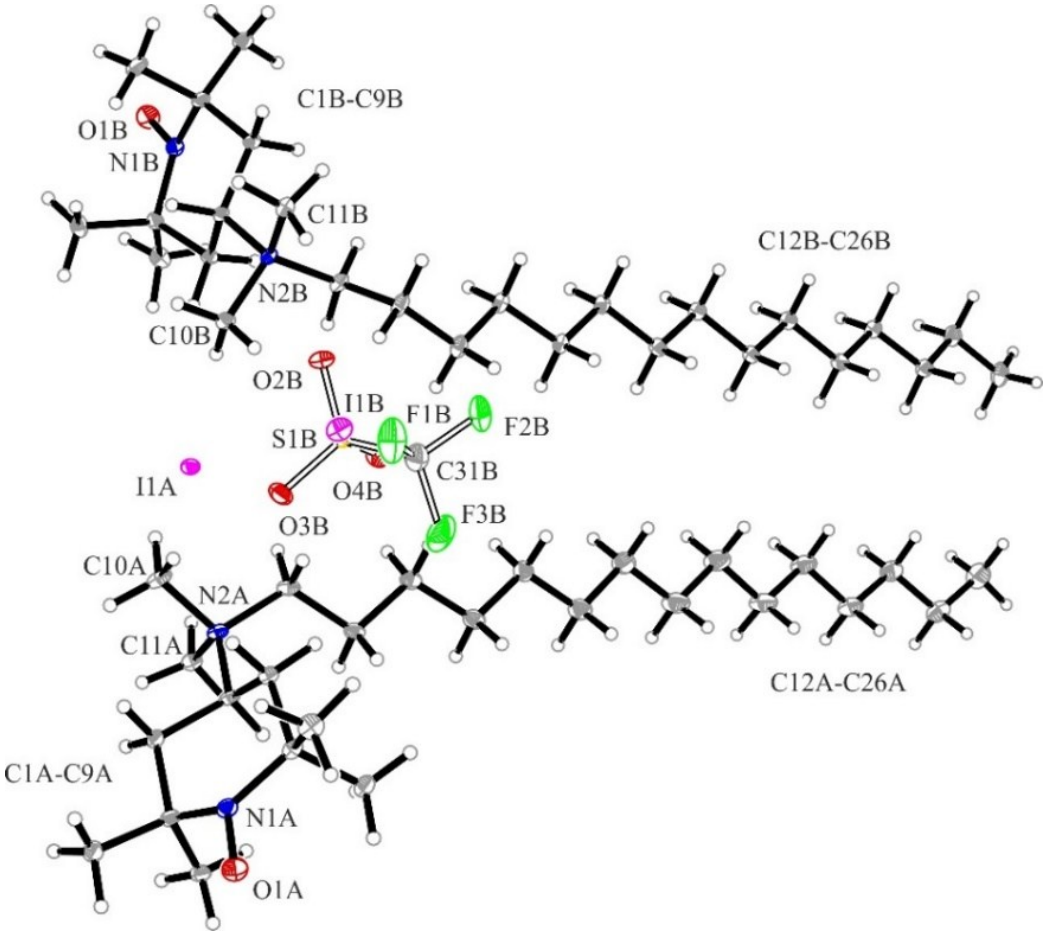

Figure S38: The asymmetric unit of **R-DMAT-15-I/OTf** containing molecule "A" [$C_{26}H_{54}N_2OI$] and molecule "B" [$C_{26}H_{54}N_2O{\cdot}I_{0.45}{\cdot}[CF_3O_3S]_{0.55}$].
Displacement ellipsoids are shown with 15% probability.

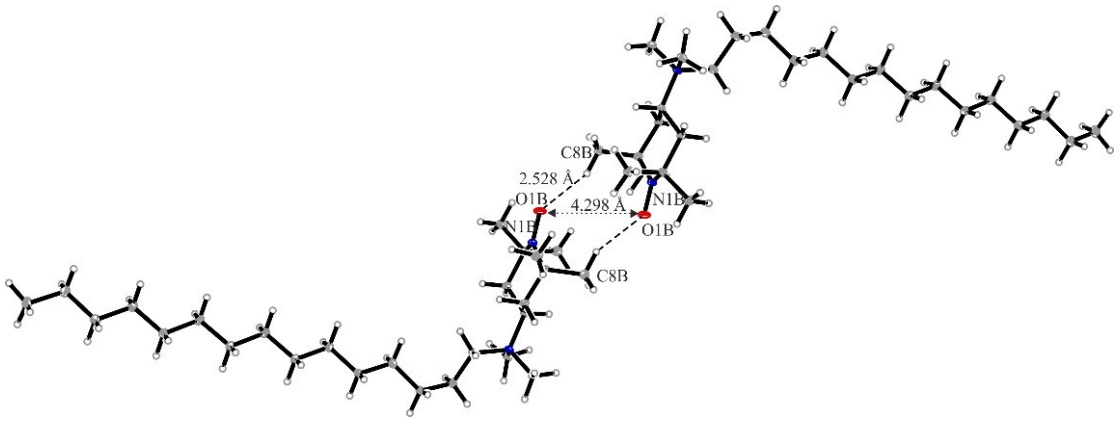

Figure S39: *S*-like shaped dimer formation between the "B" molecules involving *C-H···O* hydrogen bonds and the representation of *O1B···O1B* distance 4.298 Å in **R-DMAT-15-I/OTf**.

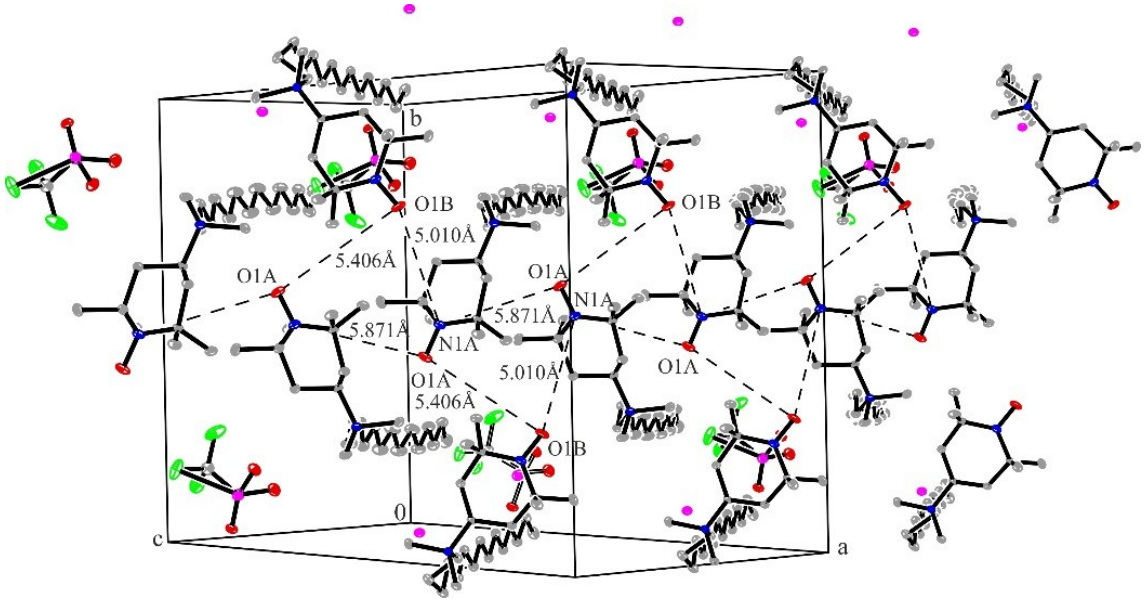

Figure S40: Packing diagram representing the *O···O* and *N···O* interactions along the *c*-axis in **R-DMAT-15-I/OTf** (*O1A···O1B* 5.406 Å; *O1A···N1A* 5.871 Å; *O1B···N1A* 5.010 Å).

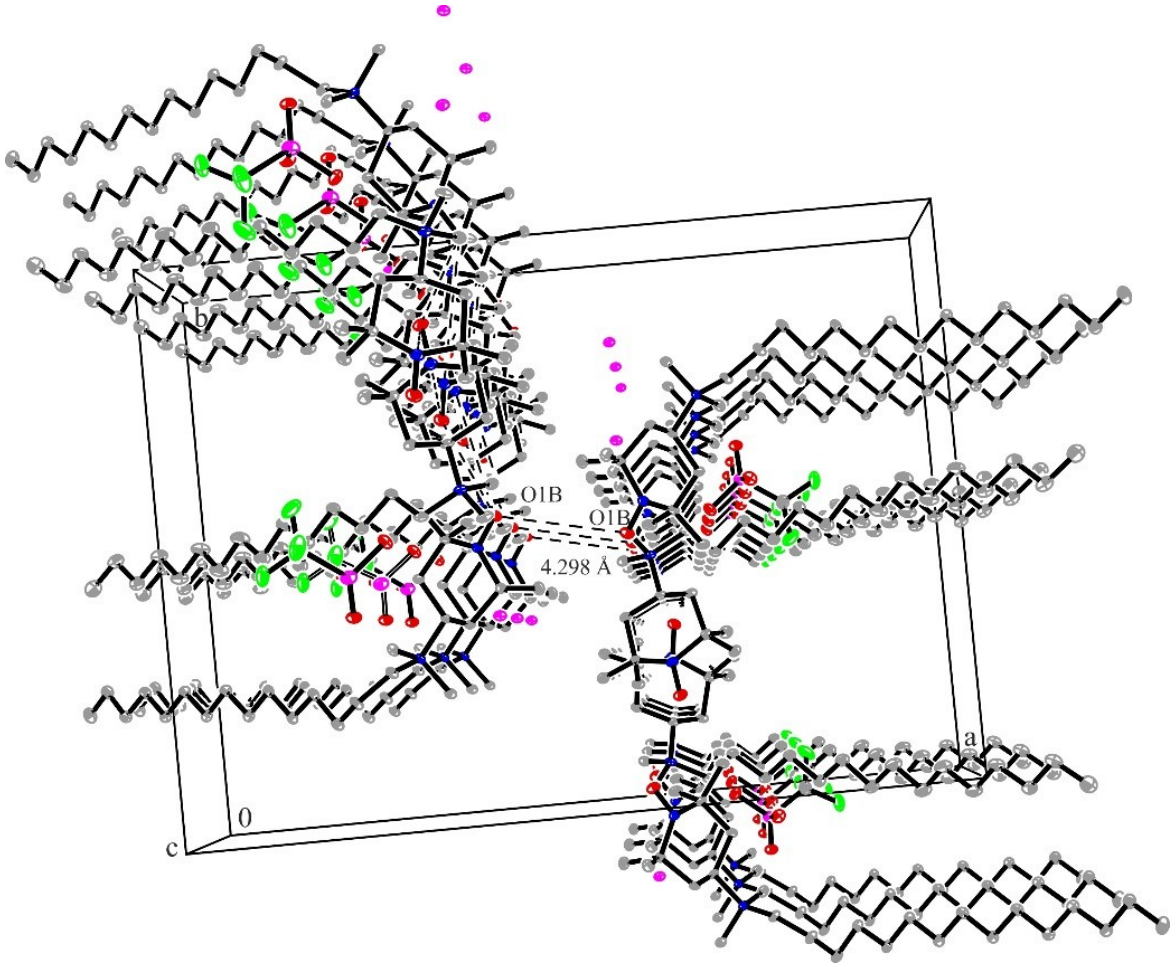

Figure S41: Formation of *S*-like shape between the “B” molecules and the *U*-like shape between the “A” molecules in the packing diagram of **R-DMAT-15-I/OTf** (*O⋯O* interactions between the “B” molecules along the *a*-axis: *O1B⋯O1B* 4.298 Å).

7.2. R-DMAT-14 Iodide/Triflate (50:50 Solid Solution)

X-ray crystal structure analysis of R-DMAT-14-I/OTf (stu8482): A colorless plate-like specimen of $2{\cdot}C_{25}H_{52}N_2O{\cdot}I_{1.50}{\cdot}[CF_3O_3S]_{0.50}$, approximate dimensions 0.010 mm x 0.200 mm x 0.200 mm, was used for the X-ray crystallographic analysis. The X-ray intensity data were measured. A total of 1525 frames were collected. The total exposure time was 30.54 h. The frames were integrated with the *Bruker SAINT* Software package using a wide-frame algorithm. The integration of the data using a monoclinic unit cell yielded a total of 53824 reflections to a maximum θ angle of 67.15° (0.84 Å resolution), of which 9794 were independent (average redundancy 5.496, completeness = 95.5%, R_{int} = 15.24%, R_{sig} = 12.72%) and 5956 (60.81%) were greater than $2\sigma(F^2)$. The final cell constants of *a* = 25.112(2) Å, *b* = 18.588(2) Å, *c* = 12.3475(13) Å, *β* = 95.627(5)°, *V* = 5735.8(10) Å^3, are based upon the refinement of the XYZ-centroids of 7417 reflections above 20 σ(I) with 5.925° < 2θ < 130.8°. Data were corrected for absorption effects using the multi-scan method (SADABS). The ratio of minimum to maximum apparent transmission was 0.598. The calculated minimum and maximum transmission coefficients (based on crystal size) are 0.334 and 0.933. The structure was solved and refined using the Bruker SHELXTL Software Package, using the space group $P2_1/c$, with $Z = 4$ for the formula unit, $2{\cdot}C_{25}H_{52}N_2O{\cdot}I_{1.50}{\cdot}[CF_3O_3S]_{0.50}$. The final anisotropic full-matrix least-squares refinement on F^2 with 611 variables converged at R1 = 7.36%, for the observed data and wR2 = 20.49% for all data. The goodness-of-fit was 1.044. The largest peak in the final difference electron density synthesis was 1.01 e$^-$/Å^3 and the largest hole was 1.20 e$^-$/Å^3 with an RMS deviation of 0.14 e$^-$/Å^3. On the basis of the final model, the calculated density was 1.23 g/cm^3 and F(000), 2256 e$^-$. CCDC Nr.: 1826204.

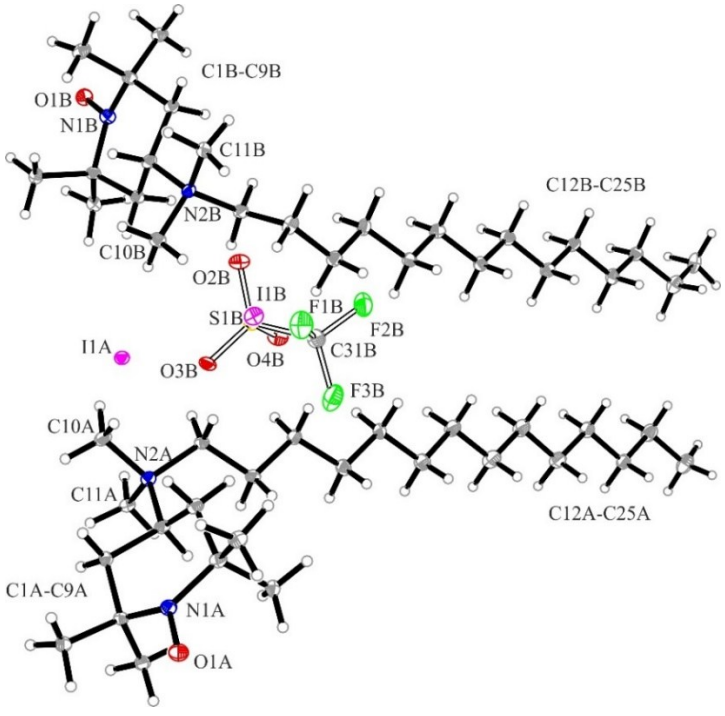

Figure S42: The asymmetric unit of **R-DMAT-14-I/OTf** containing molecule "A" [$C_{25}H_{52}N_2OI$] and molecule "B" [$C_{25}H_{52}N_2O{\cdot}I_{0.50}{\cdot}[CF_3O_3S]_{0.50}$].
Displacement ellipsoids are shown with 15% probability.

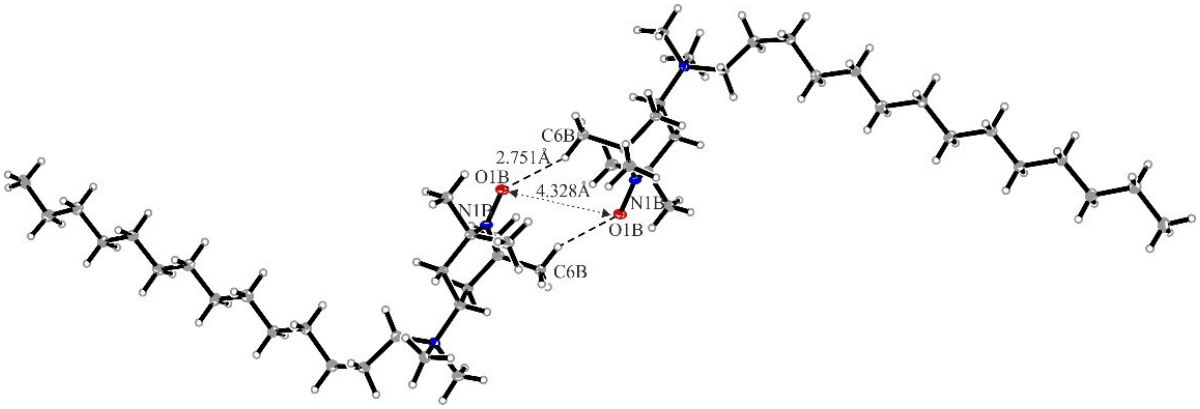

Figure S43: *S*-like shaped dimer formation between the "B" molecules involving *C-H···O* hydrogen bonds and the representation of *O1B···O1B* distance 4.328 Å in **R-DMAT-14-I/OTf**.

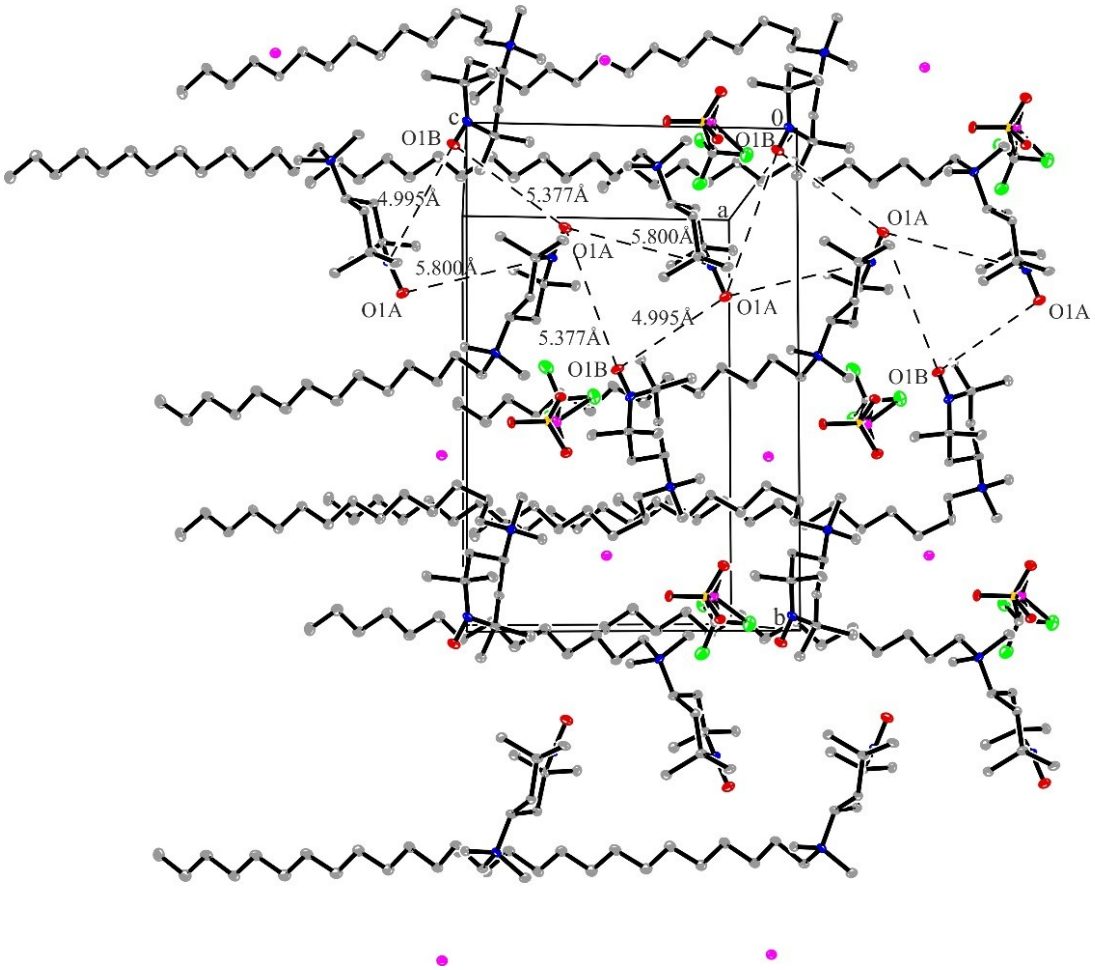

Figure S44: Packing diagram representing the *O···O* and *N···O* interactions along the *c*-axis in **R-DMAT-14-I/OTf** (*O1A···O1B* 5.377 Å; *O1A···N1A* 5.800 Å; *O1B···N1A* 4.995 Å).

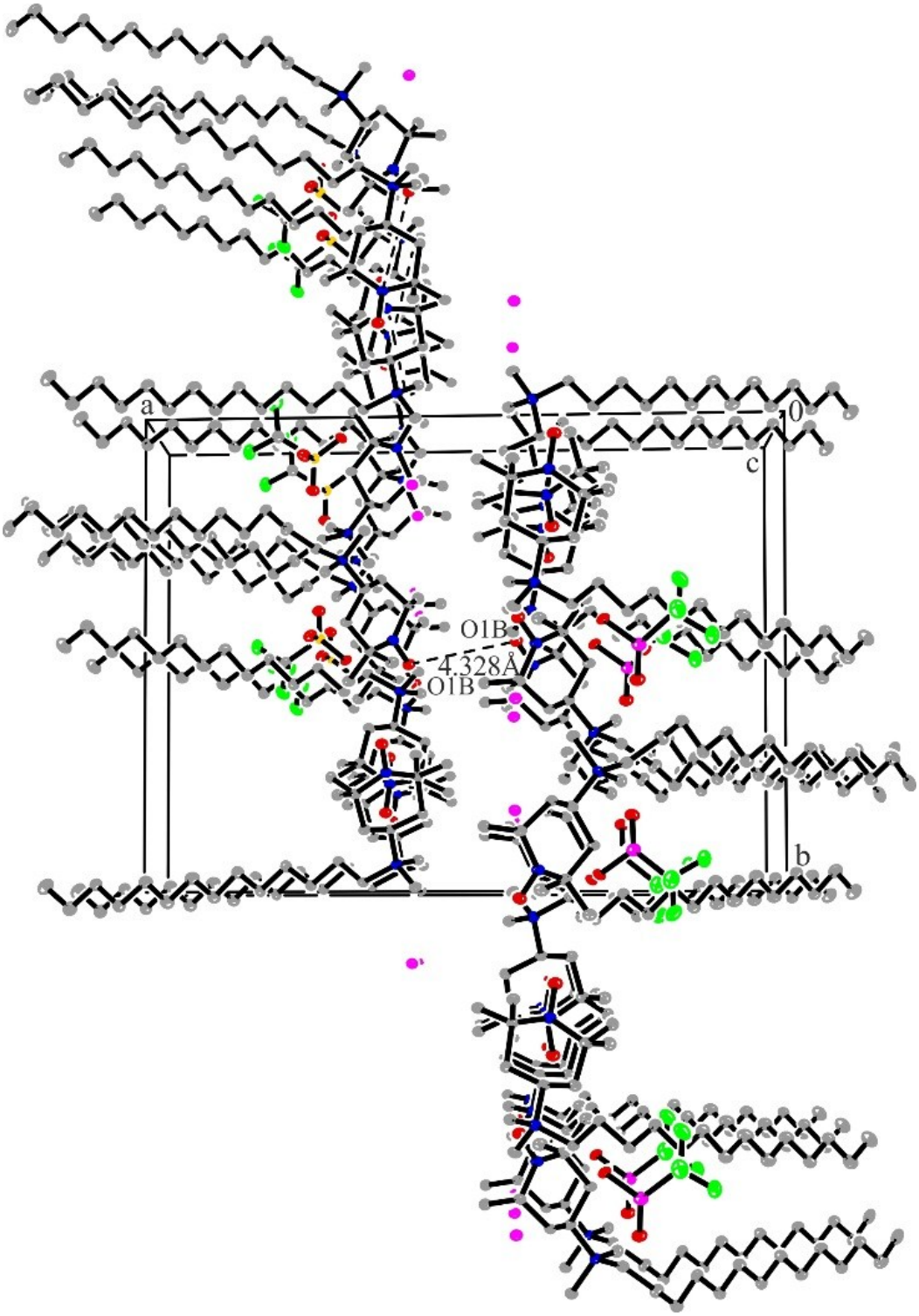

Figure S45: Formation of *S*-like shape between the "B" molecules and the *U*-like shape between the "A" molecules in the packing diagram of **R-DMAT-14-I/OTf** (*O⋯O* interactions between the "B" molecules along the *a*-axis: *O1B⋯O1B* 4.328 Å).

7.3. R-DMAT-16 Chloride

X-ray crystal structure analysis of R-DMAT16-Cl (stu8568 A yellow needle-like specimen of $C_{27}H_{56}ClN_2O \cdot 2 \times H_2O$, approximate dimensions 0.054 mm x 0.144 mm x 0.364 mm, was used for the X-ray crystallographic analysis. The X-ray intensity data were measured. A total of 928 frames were collected. The total exposure time was 18.09 h. The frames were integrated with the *Bruker SAINT* Software package using a wide-frame algorithm. The integration of the data using a monoclinic unit cell yielded a total of 28180 reflections to a maximum θ angle of 66.59° (0.84 Å resolution), of which 5221 were independent (average redundancy 5.397, completeness = 97.3%, R_{int} = 7.83%, R_{sig} = 5.90%) and 4073 (78.01%) were greater than $2\sigma(F^2)$. The final cell constants of *a* = 23.7688(8) Å, *b* = 9.2641(3) Å, *c* = 14.0543(5) Å, *β* = 100.476(2)°, *V* = 3043.12(18) Å^3, are based upon the refinement of the XYZ-centroids of 9879 reflections above 20 σ(I) with 7.564° < 2θ < 136.5°. Data were corrected for absorption effects using the multi-scan method (SADABS). The ratio of minimum to maximum apparent transmission was 0.857. The calculated minimum and maximum transmission coefficients (based on crystal size) are 0.647 and 0.933. The structure was solved and refined using the *Bruker SHELXTL* Software Package, using the space group $P2_1/c$, with Z = 4 for the formula unit, $C_{27}H_{56}ClN_2O \cdot 2 \times H_2O$. The final anisotropic full-matrix least-squares refinement on F^2 with 321 variables converged at R1 = 6.75%, for the observed data and wR2 = 12.58% for all data. The goodness-of-fit was 1.172. The largest peak in the final difference electron density synthesis was 0.25 e$^-$/Å^3 and the largest hole was 0.27 e$^-$/Å^3 with an RMS deviation of 0.06 e$^-$/Å^3. On the basis of the final model, the calculated density was 1.08 g/cm^3 and F(000), 1108 e$^-$. CCDC Nr.: 1826207.

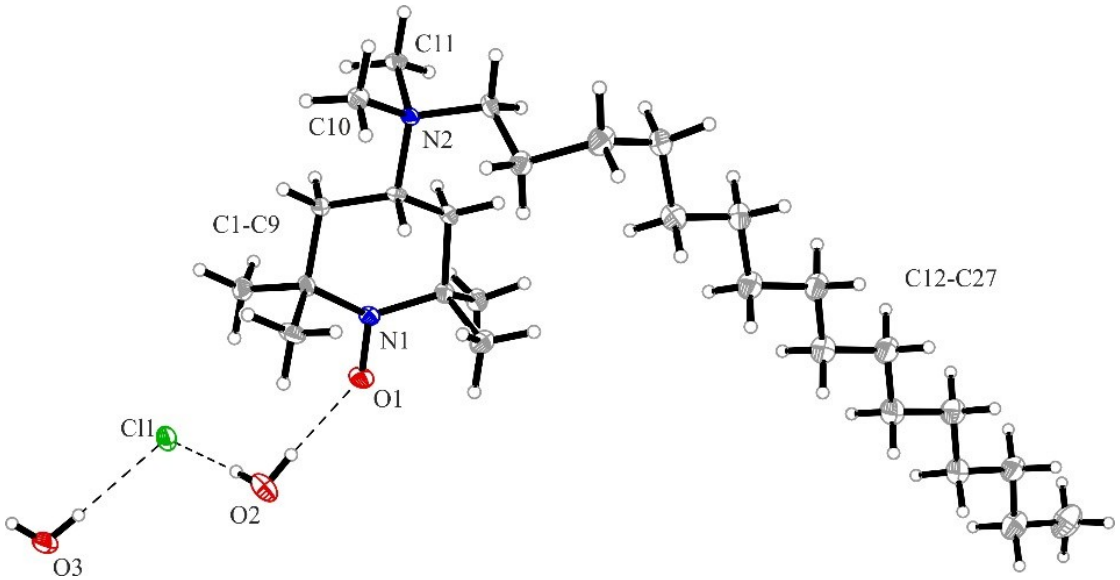

Figure S46: Asymmetric unit of **R-DMAT-16-Cl x 2 H_2O** representing the *O-H···O* and *O-H···Cl* hydrogen bonds. Displacement ellipsoids are shown with 50% probability.

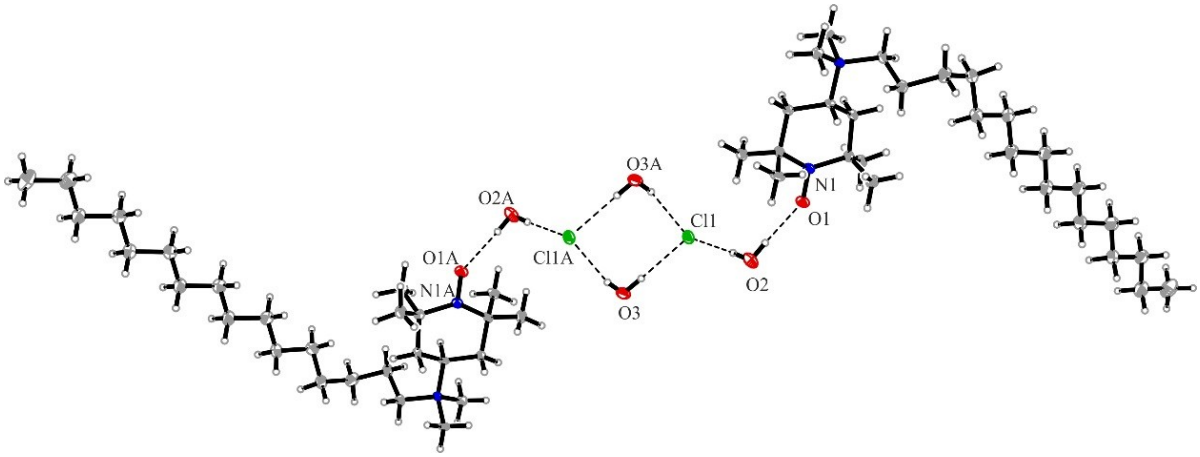

Figure S47: Dimer formation between two molecules of **R-DMAT-16- Cl · 2 H_2O** involving *O-H···O* and *O-H···Cl* hydrogen bonds; no *O1···O1* interactions were observed.

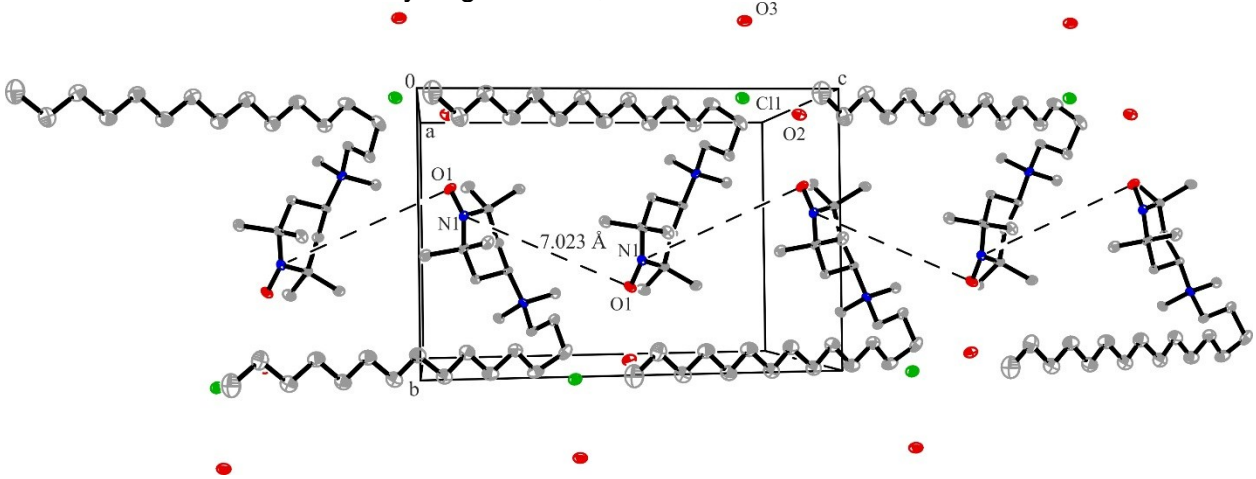

Figure S48: Packing diagram representing the *N···O* distances along the *c*-axis in **R-DMAT-16-Cl · 2 H_2O** (*O1···N1* 7.023 Å).

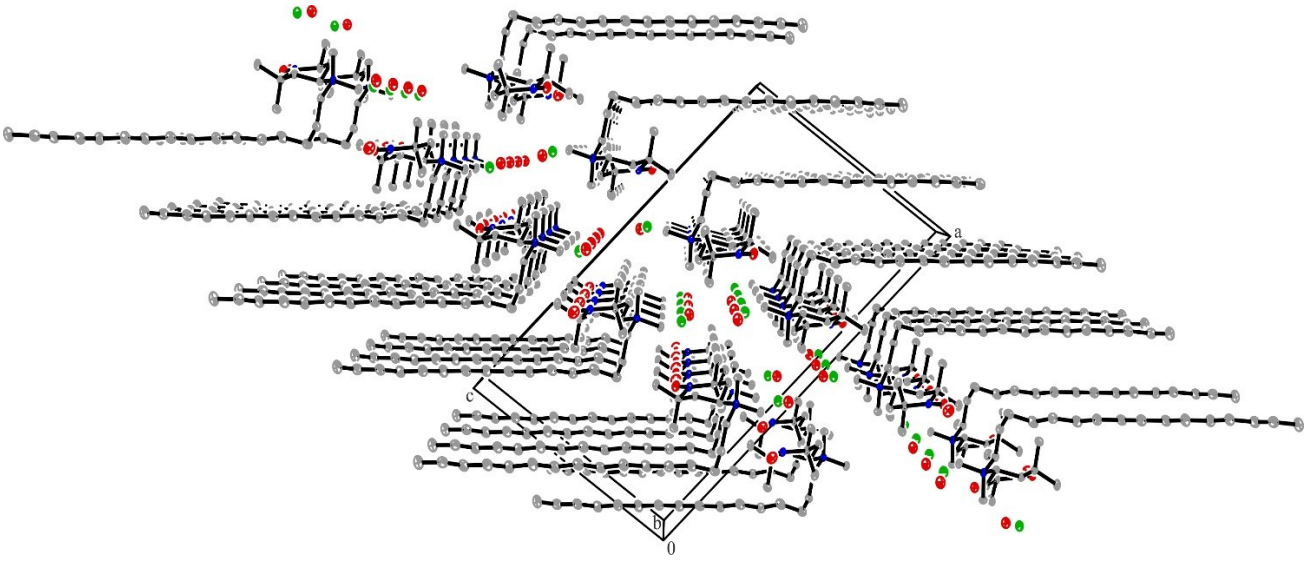

Figure S49: View perpendicular of *ac*-plane in **R-DMAT-16- Cl · 2 H_2O** packing diagram. No relevant *O···O* or *O···N* interactions were observed.

8. Literature

[1] O. Miyata, S. Takahashi, A. Tamura, M. Ueda, T. Naito, *Tetrahedron,* **2008**, *64*, 1270–1284.

[2] C. Froessl, W. Boland, *Tetrahedron,* **1993**, *49*, 6613–6618.

[3] P. Schattling, F. D. Jochum, P. Theato, *Chem. Commun.,* **2011**, *47*, 8859–8861.

[4] S. Jockusch, O. Zeika, N. Jayaraj, V. Ramamurthy, N. J. Turro, *J. Phys. Chem. Lett.,* **2010**, *1*, 2628–2632.

[5] A. Kamal, G. Ramesh, N. Laxman, *Synth. Commun.,* **2001**, *31*, 827–833.

[6] G. Cahiez, O. Gager, A. Moyeux, T. Delacroix, *Adv. Synth. Catal.,* **2012**, *354*, 1519–1528.

[7] D. Noutsias, G. Vassilikogiannakis, *Org. Lett.,* **2012**, *14*, 3565–3567.

[8] D. Pijper, E. Bulten, J. Šmisterová, A. Wagenaar, D. Hoekstra, J. B. F. N. Engberts, R. Hulst, *Eur. J. Org. Chem.,* **2003**, *2003*, 4406–4412.

[9] W. G. Dauben, D. P. Bridon, B. A. Kowalczyk, *J. Org. Chem.,* **1989**, *54*, 6101–6106.

[10] K. Kulbitski, G. Nisnevich, M. Gandelman, *Adv. Synth. Catal.,* **2011**, *353*, 1438–1442.

[11] C. Lainé, E. Mornet, L. Lemiègre, T. Montier, S. Cammas-Marion, C. Neveu, N. Carmoy, P. Lehn, T. Benvegnu, *Chem. Eur. J.,* **2008**, *14*, 8330–8340.

[12] T. Hartman, J. Šturala, R. Cibulka, *Adv. Synth. Catal.* **2015**, *357*, 3573–3586.

[13] S. Nakatsuji, A. Takai, K. Nishikawa, Y. Morimoto, N. Yasuoka, K. Suzuki, T. Enoki, H. Anzai, *J. Mater. Chem.,* **1999**, *9*, 1747–1754.

[14] T. Dresselhaus, S. Eusterwiemann, D. R. Matuschek, C. G. Daniliuc, O. Janka, R. Pöttgen, A. Studer, J. Neugebauer, *Phys. Chem. Chem. Phys*., **2016**, *18*, 28262–28273.

[15] M. Deumal, M. J. Bearpark, J. J. Novoa, M. A. Robb, *J. Phys. Chem. A,* **2002**,*106*, 1299–1315.

[16] J. J. Novoa, M. Deumal, J. Jornet-Somoza, *Chem. Soc. Rev*., **2011**, *40*, 3182–3212.

[17] L. Noodleman, *J. Chem. Phys*., **1981**, *74*, 5737–5743.

[18] F. Neese, *WIREs Com. Mol. Sci.,* **2012**, *2*, 73–78.

[19] C. Adamo, V. Barone, *J. Chem. Phys*., **1999**, *110*, 6158–6170.

[20] J. Zheng, X. Xu, D. G. Truhlar, *Theor. Chem. Acc.,* **2011**, *128*, 295–305.

[21] S.Grimme, J. Antony, S. Ehrlich, H. Krieg, *J. Chem. Phys*., **2010** 132, 154104

[22] S. Grimme, S. Ehrlich, L. Goerigk, *J. Comput. Chem*., **2011**, 32, 1456

[23] S. Aonuma, H. Casellas, C. Faulmann, B. Garreau de Bonneval, I. Malfant, P. Cassoux, P. G. Lacroix, Y. Hosokoshi, K, Inoue, *J. Mater. Chem*., **2001**,11, 337-345

[24] J. Moellmann, S. Grimme, *J. Phys. Chem. C*, **2014** 118 (14), 7615-7621